



16 **Abstract.**

17 The present analysis deals with one of the most debated aspect of the studies on the Upper
18 Troposphere/Lower Stratosphere (UTLS), namely the budget of the water vapour (H₂O) at the
19 tropical tropopause. Within the French project “Multiscale water budget in the upper
20 troposphere and lower stratosphere in the TROpics” (TRO-pico), a global-scale analysis has
21 been set up based on space-borne observations, model and assimilation techniques. The
22 MOCAGE-VALENTINA assimilation tool has been used to assimilate the Aura Microwave
23 Limb Sounder (MLS) version 3.3 H₂O measurements within the 316–5 hPa hPa range from
24 August 2011 to March 2013 with an assimilation window of 1 hour. Diagnostics are
25 developed to assess the quality of the assimilated H₂O fields depending on several
26 parameters: model error, observation minus analysis and forecast. Comparison with an
27 independent source of H₂O measurements in the UTLS based on the spaceborne Michelson
28 Interferometer for Passive Atmospheric Sounding (MIPAS) observations and with
29 meteorological ARPEGE analyses are also shown. Sensitivity studies of the analyzed fields
30 have been performed by: 1) considering periods when no MLS measurements are available
31 and 2) using another MLS version 4.2 H₂O data. The studies have been performed within 3
32 different spaces in time and space coincidences with MLS and MIPAS observations and with
33 the model outputs and at 3 different levels: 121 hPa (upper troposphere), 100 hPa
34 (tropopause), and 68 hPa (lower stratosphere) in January and February 2012. In the MLS
35 space, the analyses behave consistently with the MLS observations from the upper
36 troposphere to the lower stratosphere. In the model space, the analyses are wetter than the
37 “true” atmosphere as represented by ARPEGE and MLS in the upper troposphere (121 hPa)
38 and around the tropopause (100 hPa), but consistent with MLS and MIPAS in the lower
39 stratosphere (68 hPa). In the MIPAS space, the sensitivity and the vertical resolution of the
40 MIPAS data set at 121 and 100 hPa prevent to assess the behaviour of the analyses at 121 and



41 100 hPa particularly over intense convective areas as the Southern American, the African and
42 the Maritime continents but, in the lower stratosphere (68 hPa), the analyses are very
43 consistent with MIPAS. Sensitivity studies show the great improvement on the H₂O analyses
44 in the tropical UTLS when assimilating spaceborne measurements of better quality
45 particularly over the convective areas.

46

47



47 **1 Introduction**

48 Water is constantly cycling through the atmosphere. It evaporates from the earth's
49 surface and rises on warm updrafts into the atmosphere. Then it condenses into clouds, is
50 blown by the wind, and then falls back to the Earth's surface in form of rain or snow. This
51 cycle is one important way to transfer the heat and energy from the surface of the Earth to the
52 atmosphere, and transported from one place to another on the globe. Water vapour (H₂O) is
53 also one of the dominant greenhouse gas in the Earth's atmosphere. Unlike other greenhouse
54 gases, the additional water vapour in the atmosphere was not put there directly by humans.
55 The increase in water vapour occurs because the climate is warming, and the increase then
56 contributes to further warming. This process is referred to as a positive feedback. The effect
57 of water vapour as a greenhouse gas on climate change is a key parameter due to its positive
58 feedback on the earth radiative budget. The concentration of water vapour in the atmosphere
59 ranges from 3% of volume in wet tropical areas to a few parts per million by volume (ppmv)
60 in the stratosphere. Water vapour mixing ratio in the lower stratosphere is generally very low
61 (2.5–5.3 ppmv) (Panwar et al., 2012).

62 Brewer (1949) postulated that the observed stratospheric air must have passed through
63 the cold tropopause region observed over the tropics. The evolution of H₂O in the Upper
64 Troposphere and Lower Stratosphere (UTLS) is still not well understood irrespective of
65 numerous space- and balloon-borne data now available. One of the challenging region is the
66 tropical tropopause layer (TTL). The layer is maintained by a complex interplay between
67 large and small-scale circulation patterns, deep convection, clouds and radiation (Randel and
68 Jensen, 2013). H₂O is also a key constituent in atmospheric chemistry. It is the source of
69 hydroxyl (OH), which controls the lifetime of shorter-lived pollutants, tropospheric and
70 stratospheric ozone, and other longer-lived greenhouse gases such as methane (Seinfeld and
71 Pandis, 2006). Furthermore, H₂O has an important influence on stratospheric chemistry



72 through its ability to form ice, which offers a surface for heterogeneous chemical reactions
73 involved in the destruction of stratospheric O₃ via polar stratospheric clouds. It is noteworthy
74 that despite the importance of water vapour, there seems to be only little skill in representing
75 water vapour distributions in current chemistry-climate models specially in extratropical
76 UTLS (Hegglin et al., 2010), as well as in climate models such as used for the IPCC climate
77 assessments (Jiang et al., 2012) and reanalyses (Jiang et al., 2010) in these regions.
78 Combining models and measurements together to understand the interannual and long-term
79 behaviour of stratospheric water vapour, even in the lower stratosphere, as presented in
80 Heggling et al. (2014) can help characterizing biases in observations and also the physical
81 processes responsible for the long-term trends in water vapour.

82 The lack of progress in representing UTLS water vapour in models may partially be
83 explained by inconclusive observational records, to which the models are compared (SPARC
84 CCMVal, 2010). It is not trivial to accurately measure water vapour in the TTL, and satellite
85 measurements, as well as in situ correlative data, have been shown to exhibit large absolute
86 differences (SPARC WAVAS, 2000). In particular, the current lack of an accepted standard
87 from in situ correlative data precludes a conclusive assessment of the performance of
88 available satellite water vapour measurements (see Weinstock et al., 2009). To cope with this
89 issue, the Global Climate Observing System (GCOS) Reference Upper-Air Network
90 (GRUAN) international reference observing network has been designed to fill an important
91 gap in the current global observing system, providing long-term, high-quality climate data
92 records (including H₂O) from the surface, through the troposphere, and into the stratosphere
93 (see e.g. http://www.dwd.de/EN/research/international_programme/gruan/home.html).

94 Around the tropopause, large gradients in H₂O and interplay of transport processes
95 between troposphere and stratosphere, mainly due to rapid change in H₂O by deep
96 convection, are highly challenging for an accurate representation of H₂O in global models.



97 The most advanced Numerical Weather Prediction (NWP) models use sophisticated data
98 assimilation systems to better represent H₂O in the UTLS based on direct (e.g. radiosonde)
99 and indirect (e.g. satellite radiance) observations. For instance, at the European Centre for
100 Medium-range Forecast (ECMWF), state-of-the-art assimilation systems are operationally
101 used to provide some of the best forecasts, analyses, and reanalyses among the NWP centres
102 around the world (<http://apps.ecmwf.int/wmolcdnv/>).

103 Recently, Kunz et al. (2014) carried out a comprehensive assessment of the UTLS H₂O
104 in the most recent ECMWF analyses and reanalyses. The authors compared the operational
105 analysis and ERA-Interim reanalysis datasets to a 10-year climatology of H₂O measurements
106 in the UTLS from the Fast In Situ Stratospheric Hygrometer (FISH, Zoger et al., 1999). FISH
107 instruments have been used between 2001 and 2011 in 10 international airborne campaigns
108 from polar regions to the tropics, including the Tropical Convection, Cirrus and Nitrogen
109 Oxides Experiment (TROCCINOX) campaign in 2005 which was specifically dedicated to
110 the study of deep tropical convection (Schiller et al., 2009).

111 ERA-Interim reanalyses benefit from the 12-hour sequential 4D-Var data assimilation
112 scheme at T255 spectral resolution (80 km) and 60 hybrid levels based on the operational
113 Integrated Forecast System (IFS) (version Cy31r2) operationally used at ECMWF between
114 2006 and 2007. Note that beyond the tropopause, no direct humidity observation is
115 assimilated and all supersaturation is suppressed, which means that, in the stratosphere, the
116 humidity distribution is mainly controlled by troposphere-to-stratosphere exchange,
117 advection, and methane oxidation schemes in IFS. Specifications of the forecast model, data
118 assimilation system, and assimilated datasets are thoroughly described by Dee et al. (2011).

119 Unlike the reanalyses, which are based on a single version of the data assimilation
120 system and forecast model, the operational analyses have benefited from significant
121 modifications of the IFS and the 12-hour 4D-Var data assimilation system over the period



122 2001-2011. The changes mostly impacted H₂O fields over this period are: a revised
123 convection scheme, introduced in 2007 (Cy32r3), the better account for ice supersaturation in
124 4D-Var in 2009 (Cy35r3), and a new cloud scheme in 2010 (Cy36r4). The horizontal
125 resolution of the analyses is also higher than that of the reanalyses, with T511 spectral
126 resolution (39 km) and 61 vertical levels from 2001 to 2006, increased to T1279 (16 km) and
127 91 levels in 2010. Note that, at the present time, ECMWF high resolution model produces
128 analyses thanks to a new cubic octahedral grid of Tco1279 horizontal resolution (9 km) and
129 137 vertical levels (Cy41r2). Documentation related to model changes is available online at
130 the following address: [http://www.ecmwf.int/en/forecasts/documentation-and-](http://www.ecmwf.int/en/forecasts/documentation-and-support/changes-ecmwf-model)
131 [support/changes-ecmwf-model](http://www.ecmwf.int/en/forecasts/documentation-and-support/changes-ecmwf-model).

132 Compared to FISH measurements, about 30% of the ERA-Interim reanalyses were
133 found to be in very good agreement (deviation from the model < 10%), both in very dry and
134 very wet conditions, and another 57% have been defined as in fairly good agreement with the
135 model (deviation < 50%). Only 13% of the data were showing large positive or negative
136 biases (deviation > 50%). The authors also analyzed the data in function of their geographical
137 repartition, i.e. in the tropics, in the subtropics and in the extratropics, using the height of the
138 thermal tropopause as proxy. In the LS, at all latitudes, the deviation of FISH observations
139 from ERA-Interim is very small, which means that there is no lower stratospheric wet bias as
140 suggested in previous studies (Oikonomou and O'Neil, 2006; Luo et al., 2007; Flentje et al.,
141 2007; Schafler et al., 2010). Only the extratropical tropopause region (± 4 km around the
142 thermal tropopause) and tropical UT were shown to have deviations up to 10 times to the
143 observed values.

144 Focusing on the H₂O amount and transport from UT to LS, Jiang et al. (2015) show that
145 the reanalyses from ECMWF and from NASA Modern-Era Retrospective Analysis for
146 Research and Applications (MERRA) and its newest release (MERRA2) overestimate annual



147 global mean UT H₂O by up to ~150% compared to MLS observations. Substantial differences
148 in H₂O transport that impact on H₂O budget are also found between the observations and
149 reanalyses. H₂O transport across the tropical tropopause in the reanalyses is faster by up to
150 ~86% compared to MLS observations. In the tropical LS, the mean vertical transport from
151 ECMWF is 168% faster than the MLS estimate, while MERRA and MERRA2 have vertical
152 transport velocities within 10% of MLS values.

153 The comparison of operational analyses with FISH measurements presents similar
154 patterns. The overall good agreement is contrasted by wet biases in the extratropical
155 tropopause regions and dry bias in the tropical UT of similar order that those found in the
156 reanalyses. Nevertheless, the authors pointed out that those biases were reduced by up to a
157 factor 2 in the operational analyses towards the end of the period of study (2011) with respect
158 to ERA-Interim. This highlights the impact of the improvements of both the IFS and the
159 assimilation system. In summary, the consistent biases found both in ERA-Interim and
160 operational analyses emphasize the difficulty to properly account for dynamical processes,
161 especially deep tropical convection, in the assimilation system and model to accurately
162 represent the water vapour distribution in the UTLS.

163 The present study is intended to address one of the most debated aspects of the TTL and
164 the LS, the budget of water vapour (H₂O), and aspires to be a baseline for further studies
165 related to the “Multiscale water budget in the upper troposphere and lower stratosphere in the
166 TROpics” (TRO-pico) project (www.univ-reims.fr/TRO-pico). One of the TRO-pico aims is
167 to monitor H₂O variations in the TTL and the LS linked to deep overshooting convection
168 during field campaigns, which took place in the austral summer of 2012 and 2013 in Bauru,
169 Sao Paulo state, Brazil, involving a combination of balloon-borne, ground-based and space-
170 borne observations and modelling. TRO-pico’s objectives are to evaluate to what extent the
171 overshooting convection and involved processes contribute to the stratospheric water vapour



172 entry. Small- and medium-size balloons were launched as part of two field campaigns (2012
173 and 2013) held during the convective period in Bauru, Sao Paulo state, Brazil. Flights
174 carrying Pico-SDLA (Tunable Laser Diode Spectrometer; Durry et al., 2008) and Flash-B
175 (Yushkov et al., 1998) hygrometers were launched early morning and late evening while
176 radiosondes were launched up to 4 times a day during the most convective period. The
177 measurements, still under analysis, are matched with space-borne and model data.

178 To evaluate the local results obtained in Bauru with respect to a larger scale,
179 comparisons with climatologies were necessary. Although seasonal and annual variations of
180 H₂O have been extensively studied, few studies were devoted to the geographical and
181 temporal variability of its diurnal cycle in the TTL. In Carminati et al. (2014), the impact of
182 the continental tropical convection on the H₂O variability was debated by considering the 8-
183 year Microwave Limb Sounder (MLS) H₂O, cloud ice-water content (IWC), and temperature
184 data sets from 2005 to 2014. The interplays between these parameters and their role in the
185 water vapour variability in the TTL were highlighted separately in the northern and southern
186 tropics. The analysis from Carminati et al. (2014) adopted the Liu and Zipser (2009)
187 philosophy to discuss the difference between daytime and night-time data sets with the aim of
188 better apprehending the role of continental convection on hydrating and dehydrating
189 processes in the TTL.

190 According to Carminati et al. (2014), in the tropical upper troposphere (177 hPa),
191 continents, including the maritime continent, present the nighttime (01:30 local time, LT)
192 peak in the water vapour mixing ratio characteristic of the H₂O diurnal cycle above tropical
193 land. The western Pacific region, governed by the tropical oceanic diurnal cycle, has a
194 daytime maximum (13:30 LT). In the TTL (100 hPa) and tropical lower stratosphere (56
195 hPa), South America and Africa differ from the maritime continent and western Pacific
196 displaying a daytime maximum of H₂O. The MLS water vapour and cloud ice-water



197 observations demonstrated a clear contribution to the TTL moistening by ice crystals
198 overshooting over tropical land regions. The process was found to be much more effective in
199 the southern tropics. Deep convection is responsible for the diurnal temperature variability in
200 the same geographical areas in the lowermost stratosphere, which in turn drives the variability
201 of H₂O.

202 Following results obtained by Carminati et al. (2014), we have used the opportunity of
203 constraining CTM H₂O outputs with MLS H₂O measurements by using the assimilation
204 techniques. The present paper intends to assess the quality of the assimilated H₂O fields to
205 study troposphere to stratosphere transport in the tropics focusing on the H₂O budget. A
206 companion paper will mainly deal with the scientific implications of the assimilated fields to
207 trace the diurnal evolution of H₂O in the TTL (Carminati et al., 2016) with a temporal
208 resolution of 1 hour.

209 Meteorological analyses from ARPEGE developed at Météo-France are more
210 dehydrated in the UTLS region than the space-borne observations of the Aura Microwave
211 Limb Sounder (MLS) instrument in the UTLS by 1 to 2 ppmv (Payra et al., 2014). Within the
212 TRO-Pico project, the primary motivation of this study is to understand the dynamical and
213 chemical processes affecting the H₂O budget in the tropical UTLS for the essential role in
214 climate change through a Chemical Transport Model (CTM). The main issue is to critically
215 diagnose and improve the CTM by the assimilation technique.

216 The present paper is structured as follows. Section 2 describes the observational data
217 while section 3 presents the MOCAGE-VALENTINA assimilation system and section 4 the
218 description of the experiments. The assimilated fields are analyzed in section 5 and validated
219 in section 6. A sensitivity study is developed in section 7 and finally section 8 concludes the
220 analysis.

221



222 **2 Observations**

223 **2.1 Aura/MLS Water Vapour Observations**

224 The MLS instrument on board the NASA's Earth Observing System (EOS) Aura
225 satellite (Waters et al., 2006) provides global measurements of temperature, ice cloud, and 16
226 chemical species including water vapour from the upper troposphere to the upper stratosphere
227 (Read et al., 2007; Lambert et al. 2007). The instrument measures ~3,500 vertical profiles per
228 day in 5 spectral regions (118, 190, 240, 640 and 2500 GHz) along a sun-synchronous sub-
229 orbital track with equatorial crossings at 01:30 AM and PM local times (LT). H₂O is retrieved
230 from the 183-GHz H₂O rotational line spectrum within the 316 to 0.002 hPa pressure range.
231 The present study was conducted using MLS H₂O Level 2 Version 3.3 (hereafter referred to
232 as V3; Livesey et al., 2011) from August 2011 to March 2012. A sensitivity study has been
233 performed in section 7 comparing the analyses with MLS H₂O V3 and MLS H₂O Level 2
234 Version 4.2 (hereafter referred to as V4; Livesey et al., 2015).

235 The H₂O profiles in V3 (V4) are characterized by a vertical resolution varying from 2 to
236 3.5 km (1.3 to 3.5 km) in the 316-1 hPa pressure range, and a precision greater than 20%
237 (greater than 20%) for pressure greater than 147 hPa, 20-10% (20-7%) between 121 and 83
238 hPa, and less than 8% (less than 6%) between 68 and 1 hPa. The accuracy is greater than 15%
239 for pressure greater than 147 hPa, 12-7% between 121 and 83 hPa, and less than 9% between
240 68 and 1 hPa for both versions (Livesey et al., 2011; 2015).

241 Hurst et al. (2014) reported agreement better than 1% between the National
242 Oceanic and Atmospheric Administration (NOAA) frost point hygrometer and MLS V3
243 from 68 to 26 hPa over three tropical sites. At 83 and 100 hPa, statistically significant biases
244 of 0.1 to 0.3 ppmv (3 to 8%) were found. Upper tropospheric pressure levels of 121 and 147
245 hPa were recently investigated in Hurst et al. (2015) in the tropics showing significant biases



246 of 0.5 and 3.0 ppmv, respectively. MLS mean biases for MLS V4 are slightly smaller at 83,
247 100 and 121 hPa than for V3 (< 0.2 ppmv), but are larger at 147 hPa (~ 0.5 ppmv).

248 With a methodology approaching that of Carminati et al. (2014), we will consider in the
249 following the 3 independent vertical layers in the TTL, at 121 hPa for the upper troposphere
250 (UT), 100 hPa for the tropopause (TP), and 68 hPa for the lower stratosphere (LS). Figure 1
251 shows the monthly-averaged MLS H₂O V3 fields in the UT, TP and LS in January 2012. We
252 clearly observe the 3 different tropical regimes depending on the layer considered. Maxima of
253 H₂O are detected above the intense convective areas in the UT: Western Pacific, Africa and
254 South America, and a minimum over the Maritime Continent. Minima of H₂O are detected
255 when reaching the cold point tropopause in the TP: Western Pacific, Maritime Continent,
256 Africa and, to a lesser extent, South America. And a zonally symmetric field of H₂O is
257 measured in the LS with no imprint of convective activity from the UT or TP whatever the
258 area considered.

259 The number of measurements per $5^\circ \times 5^\circ$ bin at 100 hPa is shown Figure 2 for MLS V3
260 H₂O fields in January 2012. We note that, in general, the tropical domain (30-50
261 measurements per bin) contains fewer measurements than the high latitude domain (40-60
262 measurements per bin) because of the sun-synchronous orbit of the AURA satellite. We also
263 note that, in the tropics above South America, Africa and the Maritime Continent, the number
264 of measurements per bin is less than 30 because of the presence of clouds that impacts both
265 on the rejection of cloud-contaminated spectra and on the quality of the retrievals.

266

267 **2.2 MIPAS**

268 The limb-viewing Fourier transform spectrometer named Michelson Interferometer for
269 Passive Atmospheric Sounding (MIPAS) (Fischer et al., 2008) is onboard the ESA satellite
270 Envisat. It has been designed to operate in the mid-infrared spectral region covering five



271 spectral bands between 685 and 2410 cm^{-1} with an unapodized full spectral resolution of
272 0.025 cm^{-1} . The instrument was launched into a sun-synchronous orbit by ESA on 1 March
273 2002. It passes the Equator in a southwards direction 14.3 times each day at 10:00 local time.
274 The Envisat mission, and consequently the MIPAS instrument, ended on 08 April 2012.

275 MIPAS run predominantly in its nominal measurement mode from July 2002 until the
276 end of March 2004. Then, due to an instrument failure, it was operating with reduced spectral
277 resolution (0.0625 cm^{-1}) for the benefit of an equivalent improvement in spatial sampling.
278 The duty cycle of this so-called optimized resolution mode has been steadily increasing from
279 30% in January 2005 to 100% from December 2007 (Wetzel et al., 2013). MIPAS measures
280 at 19 tangent points; tangent altitudes are latitude-dependent from 7 to 50 km over the poles
281 and 13 to 56 km over the equator. A latitude dependent floating altitude-sampling grid is used
282 in order to follow roughly the tropopause height along the orbit with the requirement to
283 collect at least one spectrum within the troposphere but to avoid too many cloud-affected
284 spectra (Chauhan et al., 2009). The instantaneous vertical field-of-view covers 3 km, i.e.
285 oversampling is achieved in the troposphere and lower stratosphere. Due to its emission
286 sounding capability, MIPAS records spectra of the atmosphere during day and night (Stiller et
287 al., 2012). Retrieval of temperature and trace gases from the optimized-resolution nominal
288 observation mode at the Institute of Meteorology and Climate Research (IMK) at the
289 Karlsruhe Institute of Technology in cooperation with the Instituto de Astrofísica de
290 Andalucía (IAA) is described in von Clarmann et al. (2009). The retrieval is based on
291 constrained inverse modelling of limb radiances.

292 We present the results of a validation study of water vapour, version V5R_H2O_221,
293 retrieved with the IMK/IAA (Institut für Meteorologie und Klimaforschung,
294 Karlsruhe/Instituto de Astrofísica de Andalucía, Grenada) MIPAS scientific level 2 processor.
295 Only valid profiles have gone into the analysis by considering a filter visibility equal to 1.



296 The retrieval version is based on ESA level 1 spectra from version IPF 5. The MIPAS version
297 V5R_H2O_221 H₂O water vapour has a vertical resolution of 2.3 km at 20 km and 6.9 km at
298 50 km, and the horizontal resolution is 206 km at 20 km and 436 km at 40 km. Single profile
299 precisions are 0.2 ppmv at 10 km and 0.92 ppmv at 50 km (Tschanz et al., 2013).

300 Figure 1 shows the monthly-averaged MIPAS H₂O fields in the UT, TP and LS in
301 January 2012. In the UT, MLS V3 and MIPAS H₂O fields are consistent over the tropics with
302 maxima over the Eastern Pacific Ocean, the South of Africa, and the South of the Indian
303 Ocean, and minima over the Maritime Continent, whilst 2 great differences occur above the
304 Western Pacific and the South America with maxima in MLS field and minima in MIPAS
305 field. In the TP, the Maritime Continent and Africa are strongly dehydrated (~2 ppmv) in the
306 MLS V3 field whilst MIPAS H₂O field does not show any longitudinal gradient (~4 ppmv).
307 Above, in the LS, MIPAS and MLS V3 H₂O fields are very consistent with each other
308 showing a zonally symmetric field of ~4 ppmv.

309 The number of measurements per 5°×5° bin at 100 hPa is shown Figure 2 for MIPAS
310 H₂O fields in January 2012. About 10-15 measurements per bin can be retrieved within the
311 whole month, with no great differences above the continents except maybe above Africa
312 (<10). Nevertheless, the MIPAS sampling in January 2012 (~8-15 per bin) is on average
313 much less than the MLS V3 sampling (~30-60 per bin), and this, whatever the month
314 considered from September 2011 to March 2012 (not shown).

315

316 **3 The MOCAGE-VALENTINA assimilation system**

317 In this study, the global atmospheric composition is simulated using MOCAGE (Modèle
318 de Chimie Atmosphérique à Grande Echelle). It is a three-dimensional CTM developed at
319 Météo-France (Peuch et al., 1999) which covers the planetary boundary layer, the free
320 troposphere, and the stratosphere. It provides a number of optional configurations with



321 varying domain geometries and resolutions, as well as chemical and physical
322 parameterization packages. It has the flexibility to use several chemical schemes for
323 stratospheric (e.g. El Amraoui et al., 2008a) and tropospheric studies (e.g. Ricaud et al.,
324 2014), and has been validated using a large number of measurements during the
325 Intercontinental Transport of Ozone and Precursors (ICARTT/ITOP) campaign (Bousserez et
326 al., 2007).

327 MOCAGE uses a semi-Lagrangian transport scheme and includes 47 sigma-hybrid
328 vertical levels from the surface up to 5 hPa. It has a vertical resolution of about 800 m in the
329 vicinity of the tropopause and in the lower stratosphere. For our study, we have used a global
330 model configuration with an horizontal resolution of 2° both in latitude and longitude, driven
331 dynamically every 3 hours by wind, temperature, pressure, surface pressure and specific
332 humidity fields issued from ARPEGE analyses (Courtier et al., 1991). Surface anthropogenic
333 emission is prescribed using the Monitoring Atmospheric Composition and Climate (MACC)
334 emission database, and fire events are accounted for by using the Global Fire Emissions
335 Database (GFED) version 3 inventory (Randerson et al., 2013).

336 To sum up, the microphysical, the dynamical and the radiative schemes are all treated
337 by ARPEGE. MOCAGE only considers the chemical scheme. Consequently, water vapour in
338 MOCAGE is treated as a chemical species when its value is less than 10 ppmv (roughly near
339 150 hPa) otherwise it is treated as a meteorological parameter from ARPEGE. However, to
340 achieve the goal of our study, namely to constrain MOCAGE H_2O as chemical species by
341 using MLS observations, we have modified this initial treatment by enlarging the vertical
342 domain where H_2O is considered as chemical species. More precisely, we have taken the
343 pressure level of 135 hPa as a separating limit: i) for pressures greater than 135 hPa, H_2O is
344 calculated directly from ARPEGE specific humidity, and ii) for pressures less than 135 hPa,
345 the H_2O distribution is fully controlled by MOCAGE. Figure 3 gives a schematic



346 representation of the H₂O vertical profiles used in the current study. It depicts the separating
347 limit between ARPEGE constraints and MOCAGE chemical species.

348 The assimilation system used here to incorporate MLS H₂O observations in MOCAGE,
349 is the VALENTINA system, which was initially developed in the framework of the ASSET
350 (ASSimilation of Envisat daTa) project (Lahoz et al., 2007a), and has been used in numerous
351 atmospheric chemistry data assimilation studies (Massart et al., 2009; El Amraoui et al.,
352 2010; Barret et al., 2012). It is developed jointly by Météo-France and CERFACS (Centre
353 Européen de Recherche et de Formation Avancée en Calcul Scientifique). Herein, we used a
354 3D-FGAT formulation (3D-Variational in the First Guess at Appropriate Time variant; Fisher
355 and Andersson, 2001) with an assimilation window of 1 hour to assimilate MLS H₂O
356 observations. The VALENTINA system has the capability to include the effect of the
357 averaging kernel, which takes into account vertical variations of the sensitivity of the retrieval
358 to the actual H₂O mixing ratios. This technique has already produced good quality results
359 compared to independent data especially for O₃ and CO (see e.g., El Amraoui et al., 2010;
360 Claeysman et al., 2011).

361 In VALENTINA, the background error covariance matrix (B) formulation is based on
362 the diffusion equation approach (Weaver and Courtier, 2001) and can be fully specified by
363 means of a 3D standard deviation field (diagonal of B) and 3D fields of horizontal (L_x and L_y)
364 and vertical (L_z) local correlation lengths. This technique has already produced good quality
365 results compared to independent data sets, especially for O₃ and CO (see e.g., Abida et al.,
366 2016; El Amraoui et al., 2010; Claeysman et al., 2011).

367

368 **4 Description of the experiments**

369 It is worth pointing out that H₂O as a chemical species in MOCAGE (135-5 hPa
370 pressure range) is suffering from a strong systematic bias in the UTLS region, especially in



371 the tropics. Hence, in order to reduce the magnitude of this bias, we performed a relatively
372 long assimilation run of 6-month duration using MLS V3 (and also MLS V4) observations
373 from 1 August 2011 to 31 January 2012.

374 The most crucial ingredient in a variational assimilation procedure is the background
375 error covariance matrix, B , which spreads out information extracted from observations in the
376 vertical and horizontal directions in space and weights the importance of the *a priori* state.
377 For this study, we used a simple parameterization for the B matrix. The horizontal correlation
378 lengths (L_x and L_y) are taken to be homogeneous and equal to about 200 km. The vertical
379 correlation length L_z is set to one vertical model grid point. Similarly to Emili et al. (2014),
380 the background standard deviation 3D field (model error) is parameterized as a vertically
381 varying percentage of the background profile. Roughly, it is set to 45% up to 135 hPa, 35%
382 in 135-50 hPa, and to 15% in 50-5 hPa.

383 The long-run experiment is initialized on 1 August 2011 at 00:00 UTC from a
384 climatological state. In the assimilation process, only MLS H_2O measurements which are in
385 the 316-5 hPa pressure range are used (Figure 3). When taking into account MLS averaging
386 kernels in the assimilation procedure, we found unrealistic values in some regions. Hence,
387 only H_2O measurements and their associated errors are incorporated in our 3D-FGAT
388 assimilation process. Note that the MLS observations will constrain only the model in 135-5
389 hPa pressure range where H_2O is freely evolving as a chemical species. In contrast, in 316-
390 135 hPa pressure range, the information extracted from the observations is completely lost
391 each time the MOCAGE H_2O field is updated by the ARPEGE constraint (Figure 3).

392 Figure 4 shows the temporal evolution of Observations-minus-Forecast (OmF) during
393 the whole long-run assimilation experiment at three MLS pressure levels 121.15, 100, and
394 68.13 hPa. The MLS assimilated observations minus their model-equivalent values are
395 averaged over the tropics (30°S-30°N) for each hour. The model forecast is initially high



396 biased with respect to MLS observations, from about -4 ppmv at 121 hPa, about -2 ppmv at
397 100 hPa and ± 0.1 ppmv at 68 hPa on 1st August 2011. The OmF magnitude decreases
398 gradually with time over the whole long-run experiment time period. It takes about four
399 months of assimilation to reach a model forecast state with minimum values of OmF reduced
400 to: ± 0.2 ppmv at 121 hPa, ± 0.1 ppmv 100 hPa and ± 0.05 ppmv at 68 hPa by December 2011.
401 This emphasizes the extreme difficulty of constraining MOCAGE H₂O field, which is marked
402 by important biases, by assimilating only MLS measurements.

403 On 1 December 2011 at 00:00 UTC, a free model simulation (without assimilating MLS
404 observations) is performed by initializing from the obtained analysis state. The H₂O field
405 analyses is compared with those from the free run in order to quantify the corrections brought
406 by the MLS measurements in the model.

407

408 **5 The assimilated fields**

409 The analyses are produced from 1st November 2011 to 31st March 2013; however, the
410 study concentrates on monthly-averaged H₂O fields in January and February 2012. Three
411 levels will be studied in detail: 121 hPa (UT), 100 hPa (TP) and 68 hPa (LS). Because we
412 used different data sets calculated or measured at different times and locations not necessarily
413 consistent within all the data sets, the analyses will be presented within 3 spaces in time and
414 space coincidences with MLS and MIPAS observations and with the model outputs.

415

416 **5.1 Vertical profiles in the tropics**

417 In order to highlight the quality of the different data sets used in our study around the
418 tropical tropopause, Figure 5 shows the vertical profiles of zonally-averaged H₂O in January
419 2012 over the tropical UTLS (30°N–30°S) in the MLS observation space from background,
420 MLS, MIPAS, ARPEGE and the assimilated field (MLS analyses). First of all, it is noted that



421 the vertical distribution of the MLS analyses is consistent with the MLS data. The
422 background field is wetter than the MLS analyses in the UT (~1.5 ppmv at 150 hPa) and is
423 consistent with the MLS analyses in the LS above 80 hPa. The ARPEGE field although
424 wetter in the UT (~1.5 ppmv at 150 hPa) is drier than the MLS analyses around the
425 tropopause from 120 to 50 hPa with a minimum of ~2.5 ppmv at 80 hPa. Finally, it is noted
426 that the MIPAS field is drier by 1.5 ppmv than the MLS analyses below 130 hPa, wetter by 1
427 ppmv from 130 to 70 hPa, and drier by 0.5 ppmv from 70 to 40 hPa.

428 Because of the great longitudinal variability of H₂O in the tropics, we have separated all
429 the data into 4 main boxes, namely Eastern Pacific (30°S-21°N, 176°W-114°W), Southern
430 America (30°S-12°N, 86°W-30°W), Southern Africa (30°S-12°N, 2°E-46°E) and the
431 Maritime Continent (30°S-18°N, 90°E-160°E). Figure 6 shows the same fields as in Figure 5
432 but separated into the 4 above-mentioned areas. The 5 data sets show the same general
433 features, namely a wet UT, a dry LS, and an hygropause (minimum of H₂O) around the
434 tropopause whatever the box considered. Although all the data sets are consistent in the LS
435 (40-60 hPa), some differences are worthwhile discussing. Among all the 4 domains, the
436 Maritime Continent shows, on average, the wettest UT (10.5-12.5 ppmv at 140 hPa for all the
437 data sets except MIPAS), and the driest hygropause (less than 2 ppmv for ARPEGE) because
438 the tropopause is the coldest over this domain compared to all the other domains. In the UT,
439 MIPAS data is on average much drier than all the other data sets by 4-7 ppmv, except over
440 the Eastern Pacific. The fact that MIPAS behaves very differently compared to all the other
441 data sets above the Maritime Continent might be a consequence of the systematic presence of
442 clouds over this area. Since cloud contaminated spectra are discarded in the MIPAS analysis,
443 a sampling bias towards a drier atmosphere might be generated. Around the tropopause, the
444 hygropause is located either at 100 hPa (MLS and MLS analyses) or 80 hPa (ARPEGE,
445 MIPAS, background). A local maximum is systematically detected around 60 hPa over the 4



446 geographical domains in the MLS, MLS analyses and background data sets, although absent
447 in the MIPAS and ARPEGE data sets.

448

449 **5.2 Global distribution in the MLS space**

450 The data sets are now studied at global scale along 3 different pressure levels: 121 hPa
451 (UT), 100 hPa (TP) and 68 hPa (LS). In this study, we will mainly analyze the tropical band
452 (30°S-30°N). The monthly-averaged H₂O fields representative of January 2012 in the MLS
453 space (namely in time and space coincidence with the MLS observations) from the Free Run
454 (MOCAGE), ARPEGE, MLS analyses and the background are displayed in Figures 7-9 at
455 121, 100 and 68 hPa, respectively.

456 At 121 hPa (Fig. 7), all the data sets show local maxima above the South American and
457 the African continents, the Central Pacific, and the Maritime Continent, namely where
458 convective systems are the most intense and the most efficient to bring high humidity from
459 the lowermost to the uppermost troposphere. Both the Free Run and the background data sets
460 are highly hydrated with maxima around or greater than 8 ppmv whilst the MLS analyses and
461 the ARPEGE data sets show maxima of about 5-6 ppmv. ARPEGE should represent the
462 “true” world in the UT. Although all the other data sets are wetter than ARPEGE, the
463 analyses are drier than the background by about 1 ppmv consistently with the MLS data field
464 (Fig. 1), underlining the positive impact of the assimilation technique to constraint the
465 background by the observations.

466 At 100 hPa (Fig. 8), the 4 H₂O fields tend to show different behaviours. ARPEGE and
467 the analyses exhibit a dehydrated tropopause (< 3 ppmv) whilst the background shows some
468 local maxima above the continents (5-6 ppmv) and the Free Run a highly hydrated tropopause
469 with values much greater than 8 ppmv above the continent sand the Indian Ocean. The Free
470 Run, namely MOCAGE, cannot reproduce the dehydrated tropopause since it does not



471 contain any microphysical processes to transform supersaturated air into ice particles over
472 convective continental and ocean areas. The background field is not as hydrated as the Free
473 Run as a consequence of the assimilation process but is nevertheless wetter than the “true”
474 atmosphere as represented by ARPEGE. The assimilation technique efficiently constraint the
475 background by the MLS observations to produce analyses much drier by 2-3 ppmv than the
476 background fields, although slightly wetter than ARPEGE by about 1 ppmv but with
477 consistent local minima above the South American, African and Maritime continents, as in
478 MLS (Fig. 1).

479 At 68 hPa (Fig. 9), the Free Run and ARPEGE data sets strongly differ to each other but
480 also differ to MLS analyses and background with a wet atmosphere in the Free Run (5-8
481 ppmv), a dry atmosphere in ARPEGE (1-4 ppmv) and a moderately dry atmosphere in the
482 analyses and background around 4 ppmv. The Free Run data set is too much affected by the
483 tropospheric injection of wet airmasses and cannot cope with supersaturation as explained at
484 100 hPa. ARPEGE tends to systematically show a dry lower stratosphere probably because of
485 the impact of a dry bias in the meteorological soundings above the tropopause. The
486 background and the analyses are very consistent to each other and to MLS (see Fig. 1),
487 underlining the fact that the assimilation technique has produced a H₂O field very close to the
488 MLS observations.

489

490 **5.3 Global distribution in the Model space**

491 The monthly-averaged H₂O fields representative of January 2012 in the model space
492 (namely in time and space coincidence with the MOCAGE and ARPEGE outputs) from the
493 Free Run (MOCAGE), ARPEGE, MLS analyses and the background are displayed in Figures
494 10-12 at 121, 100 and 68 hPa, respectively. At 121 hPa (Fig. 10), a very wet atmosphere is
495 calculated in the Free Run, the background and the analyses with local maxima above the



496 South American, the African and the Maritime continents (> 7 ppmv) although ARPEGE and
497 MLS (Fig. 1) are much drier with local maxima of 5 and 6 ppmv, respectively. Since the
498 background and the analyses are almost identical in the model space contrarily to what has
499 been observed in the MLS space (see previous section), this means that the MLS observations
500 are too sparse both in time and space to optimally constraint the background field. In other
501 words, outside of the assimilation window and outside of the horizontal domain where MLS
502 observations are taken, the assimilation system tends to converge to a background state
503 strongly influenced by the too wet Free Run.

504 At 100 hPa (Fig. 11), the impact of the Free run to the background is less important
505 since the tropical tropopause of the background and of the analyses (4-6 ppmv) is much less
506 hydrated than the Free run tropopause (> 8 ppmv) but still wetter than both ARPEGE and
507 MLS observations (< 3 ppmv). As at 121 hPa, the background and the analyses are almost
508 identical in the model space.

509 At 68 hPa (Fig. 12), the background and the MLS analyses (~ 4 ppmv) are very
510 consistent with the MLS observations (Fig. 1), whilst ARPEGE is much drier (< 2 ppmv) and
511 the Free run is much wetter (> 6 ppmv). The assimilation system behaves nominally in the
512 lower stratosphere since the background is no longer affected by the Free Run even outside of
513 the assimilation window when and where the MLS observations are taken into account.

514

515 **6 Validation of the assimilated fields**

516 In order to validate the analyses, we have considered both the MIPAS data sets and the
517 assimilated fields in the MIPAS space (namely in time and space coincidence with the
518 MIPAS observations). The monthly-averaged H_2O fields representative of January 2012 in
519 the MIPAS space from the Free Run (MOCAGE), ARPEGE, MLS analyses and the
520 background are displayed in Figures 13-15 at 121, 100 and 68 hPa, respectively. At 121 hPa



521 (Fig. 13), as in the model space, the analyses show a very wet upper troposphere (> 8 ppmv)
522 above the continents consistently with the background and the Free run, but in contrast to
523 ARPEGE (local maxima of 6 ppmv) and MIPAS observations (Fig. 1, maxima of ~ 7 ppmv).
524 It nevertheless seems that the MIPAS observations above convective areas (Southern
525 America, Africa and the Maritime continent) are dry biased compared to MLS observations
526 (as already discussed in section 2.2). This is probably due to the impact of the cloud presence
527 in the line of sight diminishing the number of available observations (see Fig. 2). Indeed,
528 MLS microwave observations are in general less affected by clouds than the MIPAS IR
529 observations, consequently the MIPAS H₂O field is given in a cloud-free atmosphere. The
530 MLS and MIPAS measurements occur at two different local times (01:40 am/pm for MLS
531 and 10:00 am/pm for MIPAS). Because of the diurnal cycle of the convective activity (Liu
532 and Zipser, 2009) that differs above ocean (maximum in local morning) and continents
533 (maximum in local afternoon), the MIPAS observations are probably more affected by upper
534 tropospheric clouds than the MLS observations, both over the continent and the ocean.
535 Chauhan et al. (2009) and Montoux et al. (2009) tried to clarify this cloud issue by different
536 approaches but could not clearly identify a consistent picture except the strong effects of
537 clouds within the presented comparison. They also suggested that the observed H₂O
538 variability may be contaminated by the presence of clouds in the UTLS. Another issue is the
539 altitude resolution of the MIPAS retrievals (Milz et al., 2005) in the lowermost layers at 121
540 and 100 hPa that may be too coarse (4.5-6.5 km) to allow a direct comparison without
541 application of averaging kernels.

542 At 100 hPa (Fig. 14), the analyses are very consistent with the MIPAS observations
543 (Fig. 1, ~ 4 ppmv) except above the South American, the African and the Maritime continents
544 where the analyses are wetter by 1-2 ppmv. The background and the analyses are identical
545 and differ from the wet Free run (> 8 ppmv) and the dry ARPEGE (< 2 ppmv) tropopause.



546 The dehydration observed by MLS (Fig. 1) and by ARPEGE above the Maritime Continent is
547 not reproduced by the analyses, probably because the Free run is far too wet (> 8 ppmv)
548 above this area and the assimilation system cannot cope with such a difference with the sparse
549 MLS observations.

550 At 68 hPa (Fig. 15), the analyses and the background are very consistent with the
551 MIPAS observations (~ 4 ppmv) with no longitudinal gradient although the Free run and
552 ARPEGE are wetter (~ 7 ppmv) and drier (< 2 ppmv), respectively. This tends to show that
553 the assimilation system is working properly in the lower stratosphere, despite the fact that the
554 MLS observations are sparse both in time and space.

555 To summarize, in the MLS space, the analyses behave consistently with the MLS
556 observations from the upper troposphere to the lower stratosphere (121-68 hPa). In the model
557 space, the analyses are wetter than the “true” atmosphere as represented by ARPEGE and
558 MLS in the upper troposphere (121 hPa) and around the tropopause (100 hPa) but consistent
559 with MLS and MIPAS in the lower stratosphere. In the MIPAS space, the sensitivity and the
560 vertical resolution of the MIPAS data set at 121 and 100 hPa prevent to assess the behaviour
561 of the analyses particularly over intense convective areas as the Southern American, the
562 African and the Maritime continents but, in the lower stratosphere (68 hPa), the analyses are
563 very consistent with MIPAS.

564

565 **7 Sensitivity studies**

566 We have used the opportunity of getting two versions of the MLS data to check the
567 sensitivity of the assimilation technique to this parameter that affects both the quality of the
568 data and the number of data available. But before, we have investigated the impact of some
569 periods with no measurements onto the assimilated fields induced by the fact that, in this
570 configuration, the background returns back to the Free run.



571

572 **7.1 Periods with no measurements**

573 We have already noticed that the H₂O analyses in the tropical UTLS in the model and
574 the MIPAS spaces were very sensitive to the background and consequently to the Free run
575 producing an atmosphere in the upper troposphere and in the tropopause wetter than in the
576 MLS space. We investigate here the impact of periods of no MLS measurements on the H₂O
577 analyses during the assimilation time frame of one month. Two consecutive months are very
578 interesting to consider. In January 2012, MLS has been operating nominally and 31 days of
579 measurements are available for the assimilation study. At the opposite, in February 2012, 4
580 days of measurements were unavailable, thus the assimilation process used MLS data over
581 the time frame: 1-19 and 24-29 February.

582 The relative difference between the monthly-averaged H₂O fields from the observations
583 and the assimilation in January and in February 2012 at 121, 100 and 68 hPa is shown in
584 Figure 16. The impact of the missing data in February 2012 on the analyses compared to the
585 January 2012 is clearly depicted since the Observation-minus-Analysis is, in absolute, greater
586 in February than in January: -6% vs. -4% at 121 hPa, +4% vs. +2% at 100 hPa and -2% vs.
587 +1% at 68 hPa in February vs. January 2012, respectively. When the MLS data are no longer
588 available, the background field tends to be redirected towards the Free run, losing the
589 memory of the MLS-driving information injected in the assimilation system.

590

591 **7.2 Improvement of the data quality**

592 In this section, we investigated the impact of using two versions of the MLS data on the
593 assimilation fields because the version affects both the quality of the data and the number of
594 data available. The MLS V3 and V4 are presented in section 2.1. Official documentation
595 (Livesey et al., 2015) indicates an improvement in the cloud screening and first guess



596 estimation from V3 to V4, which yielded better agreements with truth in simulation studies.
597 As an example, Figure 17 shows for January 2012 the number of measurements per $5^{\circ} \times 5^{\circ}$ bin
598 considering the MLS V4 data and the difference between the V4 and the V3 data. In the
599 tropics, the number of measurements per bin in V4 is about 15 measurements per bin more
600 than in V3, particularly over the Southern American, the African and the Maritime continents,
601 and the Indian Ocean. This clearly shows a change both in the cloud treatment and in the data
602 quality of V4 compared to V3.

603 In a similar way as performed with the MLS V3, the assimilation process has thus been
604 conducted with the MLS V4 data from 1st November 2011 to 31st March 2013, namely with
605 a background error set to 45% up to 135 hPa, 35% in 135-50 hPa, and to 15% in 50-5 hPa
606 (see section 4 for the other parameters). The monthly-averaged analyses in January 2012 at
607 121, 100 and 68 hPa are presented in Figures 18-20 in the MLS, model and MIPAS spaces,
608 respectively together with the difference between the V4 and the V3 analyses. In the MLS
609 space (Fig. 18), both versions show the same structures (maxima at 121 hPa and minima at
610 100 hPa over the convective areas) in the upper troposphere and the tropopause whilst a
611 zonally-symmetric field is detected in the tropical band in the lower stratosphere (68 hPa).
612 However, V4 analyses compared to V3 analyses tends to show a much wetter atmosphere in
613 the tropical upper troposphere and lower stratosphere by 10% and 15%, respectively and, at
614 the tropopause, a slightly drier atmosphere by 2-3%. Consequently, the difference in the
615 analyses between the two versions in the tropics is only significant at 121 and 68 hPa i.e.
616 greater than the minimum measurable value of 0.1 ppmv estimated in Livesey et al. (2011,
617 2015).

618 In the model space (Fig. 19), the two analyses behave differently depending on the level
619 and the area considered. Above the convective areas such as the Southern American, the
620 African and the Maritime continents, the atmosphere is much drier in V4 compared to V3 by



621 10%, 20% and 5% at 121, 100 and 68 hPa, respectively. Outside of these convective areas,
622 the V4 compared to the V3 atmosphere is wetter by 10% at 121 hPa, and drier by about 5-
623 10% at 100 and 68 hPa. This clearly shows the impact of V4 quality induced by cloud-
624 screening methodology on the analyses over convective areas where the presence of clouds is
625 prominent. Finally, in the MIPAS space (Fig. 20), the conclusions drawn for the model space
626 are mainly the same: V4 analyses drier than V3 above the convective areas at the 3 levels
627 considered and, outside of the convective areas, wetter V4 analyses at 121 hPa and drier
628 above.

629

630 **8 Conclusions**

631 Water vapour (H_2O) in the tropical UTLS is known to play an important role in many
632 aspects of meteorology, including radiation, dynamics, chemistry and climate change.
633 Modelling of water in the UTLS is very challenging because it varies in space and time due to
634 its rapid phase change (liquid, solid and gas). The representation of H_2O in the tropical UTLS
635 from observations and from models does not necessarily converge since some caveats are
636 detectable that impact on the measured or calculated H_2O fields, e.g. presence of clouds, in
637 the observation, cloud microphysics in the model.

638 Within the French project “Multiscale water budget in the upper troposphere and lower
639 stratosphere in the TROpics” (TRO-pico), a global-scale analysis has been set up based on
640 space-borne measurements, model and assimilation techniques to study the time evolution of
641 H_2O in the tropical UTLS. The MOCAGE-VALENTINA assimilation tool has been used to
642 assimilate the Aura MLS version 3.3 H_2O measurements within the 316-5 hPa range with an
643 assimilation window of 1 hour. The time period spans from 1st August 2011 to 31st March
644 2013 but the study concentrates on monthly-averaged H_2O fields in January and February
645 2012. Some diagnostics have been developed to assess the quality of the assimilated H_2O



646 fields depending on several parameters: model error, observation minus analysis and
647 observation minus forecast. As a validation exercise, comparisons with 2 independent sources
648 of H₂O in the UTLS have been performed based on the spaceborne MIPAS measurements
649 and on the meteorological ARPEGE analyses. Sensitivity studies of the analyzed fields have
650 been done 1) considering periods when no MLS measurements are available and 2) using
651 another MLS version 4.2 H₂O data. The studies have been performed within 3 different
652 spaces in time and space coincidences with the MLS and MIPAS observations and with the
653 model outputs and at 3 different levels: 121 hPa (upper troposphere), 100 hPa (tropopause),
654 and 68 hPa (lower stratosphere).

655 In the MLS space, the analyses behave consistently with the MLS observations from the
656 upper troposphere to the lower stratosphere. In the model space, the analyses are wetter than
657 the “true” atmosphere as represented by ARPEGE and MLS in the upper troposphere (121
658 hPa) and around the tropopause (100 hPa) but consistent with MLS and MIPAS in the lower
659 stratosphere. In the MIPAS space, the sensitivity and the vertical resolution of the MIPAS
660 data set at 121 and 100 hPa prevent to assess the behaviour of the analyses particularly over
661 intense convective areas as the Southern American, the African and the Maritime continents
662 but, in the lower stratosphere (68 hPa), the analyses are very consistent with MIPAS.
663 Sensitivity studies show the great improvement on the H₂O analyses in the tropical UTLS
664 when assimilating spaceborne measurements of better quality particularly over the convective
665 areas.

666 The analyses obtained from November 2011 (August-October 2011 is considered as a
667 spin-up period) to March 2013 are being used to assess the impact of the continental
668 convective activity on the diurnal cycle of H₂O in the tropical UTLS above the Southern
669 American continent (Carminati et al., 2016) with a temporal resolution of 1 hour. The same
670 methodology could be employed over the Indian Ocean, the Maritime continent and the



671 Tibetan Plateau to quantify the impact of the cyclone, the maritime convection and the
672 continental convection processes, respectively on the H₂O budget in the UTLS.

673

674 **Acknowledgements.** The work was supported by the French Agence Nationale de la
675 Recherche (ANR) TRO-pico project (<http://www.univ-reims.fr/TRO-pico/>). The data used in
676 this study were acquired as part of the activities of NASA's Science Mission Directorate, and
677 are archived and distributed by the Goddard Earth Sciences (GES) Data and Information
678 Services Center (DISC). The provision of MIPAS data by ESA is gratefully acknowledged.

679



679 **References**

- 680 Abida, R., J.-L. Attié, L. El Amraoui, P. Ricaud, W. Lahoz, H. Eskes, A. Segers, L. Curier, J.
681 de Haan, J. Kujanpää, A. O. Nijhuis, D. Schuettemeyer, J. Tamminen, R. Timmermans,
682 P. Veefkind, and B. Veihelmann, Impact of Spaceborne Carbon Monoxide Observations
683 from the S-5P platform on Tropospheric Composition Analyses and Forecasts, Atmos.
684 Chem. Phys. Discuss., doi:10.5194/acp-2015-924, 2016.
- 685 Bencherif, H., El Amraoui, L., Kirgis, G., Bellevue, J. L. D., Hauchecorne, A., Mz,
686 N.,Portafaix, T., Pazmino, A., and Goutail, F.: Analysis of a rapid increase of
687 stratospheric ozone during late austral summer 2008 over Kerguelen (49.4° S, 70.3° E),
688 Atmos. Chem. Phys., 11, 363–373, doi:10.5194/acp-11-363-2011, www.atmos-chem-
689 phys.net/11/363/2011/, 2011.
- 690 Brewer, A. W. (1949). Evidence for a world circulation provided by the measurements of
691 helium and water vapour distribution in the stratosphere. Quarterly Journal of the Royal
692 Meteorological Society, 75(326), 351-363.
- 693 Carminati, F., Ricaud, P., Pommereau, J.-P., Rivière, E., Khaykin, S., Attié, J.-L., and
694 Warner, J.: Impact of tropical land convection on the water vapour budget in the tropical
695 tropopause layer, Atmos. Chem. Phys., 14, 6195-6211, doi:10.5194/acp-14-6195-2014,
696 2014.
- 697 Carminati, F., P. Ricaud, J.-P. Pommereau, E. D. Rivière, J.-L. Attié, S. Payra, L. El Amraoui
698 and R. Abida, Role of saturation in the water vapor diurnal cycle in the South American
699 Tropical Tropopause Layer, to be submitted to Geophysical Research Letters, 2016.
- 700 Chauhan, S., Hopfner, M., Stiller, G. P., von Clarmann, T., Funke, B., Glatthor, N.,
701 Grabowski, U., Linden, A., Kellmann, S., Milz, M., Steck, T., Fischer, H., Froidevaux, L.,
702 Lambert, A., Santee, M. L., Schwartz, M., Read, W. G., and Livesey, N. J.: MIPAS
703 reduced spectral resolution UTLS-1 mode measurements of temperature, O₃, HNO₃,



- 704 N₂O, H₂O and relative humidity over ice: retrievals and comparison to MLS, Atmos.
705 Meas. Tech., 2, 337– 353, doi:10.5194/amt-2-337-2009, 2009.
- 706 Claeysman, M., Attie, J.-L., Peuch, V.-H., El Amraoui, L., Lahoz, W. A., Josse, B., Ricaud, P.,
707 von Clarmann, T., Hopfner, M., Orphal, J., Flaud, J.-M., Edwards, D. P., Chance, K.,
708 Liu, X., Pasternak, F., and Cantie, R.: A geostationary thermal infrared sensor to
709 monitor the lowermost troposphere: O₃ and CO retrieval studies, Atmos. Meas. Tech.,
710 4, 297–317, doi:10.5194/amt-4-297-2011, www.atmos-meas-tech.net/4/297/2011/,
711 2011.
- 712 Courtier, P., Freydier, C., Geleyn, J., Rabier, F., and Rochas, M.: The ARPEGE project at
713 Meteo France, in: Atmospheric Models, vol.2, pp. 193–231, Workshop on Numerical
714 Methods, Reading, U.K., 1991.
- 715 Dee, D. P., Uppala, S. M., Simmons, A. J., Berrisford, P., Poli, P., Kobayashi, S., Andrae, U.,
716 Balmaseda, M. A., Balsamo, G., Bauer, P., Bechtold, P., Beljaars, A. C. M., van de
717 Berg, L., Bidlot, J., Bormann, N., Delsol, C., Dragani, R., Fuentes, M., Geer, A. J.,
718 Haimberger, L., Healy, S. B., Hersbach, H., Hólm, E. V., Isaksen, L., Kållberg, P.,
719 Köhler, M., Matricardi, M., McNally, A. P., Monge-Sanz, B. M., Morcrette, J.-J., Park,
720 B.-K., Peubey, C., de Rosnay, P., Tavolato, C., Thépaut, J.-N., Vitart, F.: The ERA-
721 Interim reanalysis: configuration and performance of the data assimilation system.
722 Quarterly Journal of the Royal Meteorological Society, 137(656), 10.1002/qj.828, 553-
723 597, 2011.
- 724 Durry, G., Amarouche, N., Joly, L., Liu, X., Parvitte, B., and Zéninari, V.: Laser diode
725 spectroscopy of H₂O at 2.63 μm for atmospheric applications, Appl. Phys. B, 90, 573–
726 580, 2008.
- 727 El Amraoui, L., Peuch, V.-H., Ricaud, P., Massart, S., Semane, N., Teyss` dre, H., Cariolle,
728 D., and Karcher, F.: Ozone loss in the 2002–2003 Arctic vortex deduced from the



- 729 assimilation of Odin/SMR O₃ and N₂O measurements: N₂O as a dynamical tracer,
730 Quart. J. Roy. Meteor. Soc., 134, 217–228, 2008a.
- 731 El Amraoui, L., Semane, N., Peuch, V.-H., and Santee, M. L.: Investigation of dynamical
732 processes in the polar stratospheric vortex during the unusually cold winter 2004/2005,
733 Geophys. Res. Lett., 35, L03803, doi:10.1029/2007GL031251, 2008b.
- 734 El Amraoui, L., Attié, J.-L., Semane, N., Claeysman, M., Peuch, V.-H., Warner, J., Ricaud,
735 P., Cammas, J.-P., Piacentini, A., Josse, B., Cariolle, D., Massart, S., and Bencherif, H.:
736 Midlatitude stratosphere–troposphere exchange as diagnosed by MLS O₃ and MOPITT
737 CO assimilated fields, Atmos. Chem. Phys., 10, 2175–2194, doi:10.5194/acp-10-2175-
738 2010, <http://www.atmos-chem-phys.net/10/2175/2010/>, 2010.
- 739 Emili, E., Barret, B., Massart, S., Le Flochmoen, E., Piacentini, A., El Amraoui, L.,
740 Pannekoucke, O., and Cariolle, D.: Combined assimilation of IASI and MLS
741 observations to constrain tropospheric and stratospheric ozone in a global chemical
742 transport model, Atmos. Chem. Phys., 14, 177–198, doi:10.5194/acp-14-177-2014,
743 2014.
- 744 Fischer, H., Birk, M., Blom, C., Carli, B., Carlotti, M., von Clarmann, T., Delbouille, L.,
745 Dudhia, A., Ehhalt, D., Endemann, M., Flaud, J. M., Gessner, R., Kleinert, A.,
746 Koopman, R., Langen, J., Lopez-Puertas, M., Mosner, P., Nett, H., Oelhaf, H., Perron,
747 G., Remedios, J., Ridolfi, M., Stiller, G., and Zander, R.: MIPAS: an instrument for
748 atmospheric and climate research, Atmos. Chem. Phys., 8, 2151–2188, doi:10.5194/acp-
749 8-2151-2008, 2008.
- 750 Flentje, H., Dörnbrack, A., Fix, A., Ehret, G. and Hólm, E.: Evaluation of ECMWF water
751 vapour fields by airborne differential absorption lidar measurements: a case study
752 between Brazil and Europe. Atmos. Chem. Phys., 7, 5033–5042, 2007.



- 753 Froidevaux, L., N. J. Livesey, W. G. Read, Y. B. Jiang, C. Jimenez, M. J. Filipiak, M. J.
754 Schwartz, M. L. Santee, H. C. Pumphrey, J. H. Jiang, D. L. Wu, G. L. Manney, B. J.
755 Drouin, J. W. Waters, E. J. Fetzer, P. F. Bernath, C. D. Boone, K. A. Walker, K. W.
756 Jucks, G. C. Toon, J. J. Margitan, B. Sen, C. R. Webster, L. E. Christensen, J. W.
757 Elkins, E. Atlas, R. A. Lueb, and R. Hendershot, 2006: Early validation analyses of
758 atmospheric profiles from EOS MLS on the AURA satellite. *IEEE Trans. Geosci.*
759 *Remote Sensing*, 44, 1106-1121, doi: 10.1109/TGRS.2006.864366.
- 760 Hegglin, M. I., et al., Multimodel assessment of the upper troposphere and lower stratosphere:
761 Extratropics, *J. Geophys. Res.*, 115, D00M09, doi:10.1029/2010JD013884, 2010.
- 762 Hegglin, M.I., Plummer, D.A., Shepherd, T.G., Scinocca, J.F., Anderson, J., Froidevaux, L.,
763 Funke, B., Hurst, D., Rozanov, A., Urban, J. and von Clarmann, T.: Vertical structure of
764 stratospheric water vapour trends derived from merged satellite data, *Nature*
765 *Geoscience*, 7, 768-776. doi:10.1038/ngeo2236, 2014.
- 766 Hurst, D. F., Lambert, A., Read, W. G., Davis, S. M., Rosenlof, K. H., Hall, E. G., Jordan, A.
767 F., Oltmans, S. J.: Validation of Aura Microwave Limb Sounder stratospheric water
768 vapor measurements by the NOAA frost point hygrometer, *Journal of Geophysical*
769 *Research: Atmospheres*, 119, 1612-1625, 2014.
- 770 Hurst, D. et al.: Water Vapor Measurement Biases in the TTL: MLS vs Frost Point
771 Hygrometers, in: CT3LS meeting, Boulder, Colorado, URL
772 <http://esrl.noaa.gov/csd/events/CT3LS/presentations/wed-posters-4-hurst.pdf>, 2015.
- 773 Ide, K., Courtier, P., Ghil, M., & Lorenc, A. C. (1997). Uni ed notation for data assimilation:
774 operational, sequential and variational. *Practice*, 75(1B), 181-189.
- 775 Jiang, J. H., et al.: Five year (2004–2009) observations of upper tropospheric water vapor and
776 cloud ice from MLS and comparisons with GEOS-5 analyses, *J. Geophys. Res.*, 115,
777 D15103, doi:10.1029/2009JD013256, 2010.



- 778 Jiang, J. H., et al.: Evaluation of cloud and water vapor simulations in CMIP5 climate models
779 using NASA “A-Train” satellite observations, *J. Geophys. Res.*, 117, D14105,
780 doi:10.1029/2011JD017237, 2012.
- 781 Jiang, J. H., Su, H., Zhai, C., Wu, L., Minschwaner, K., Molod, A. M., and Tompkins, A. M.:
782 An assessment of upper troposphere and lower stratosphere water vapor in MERRA,
783 MERRA2, and ECMWF reanalyses using Aura MLS observations, *Journal of*
784 *Geophysical Research: Atmospheres*, 120, 2015.
- 785 Kunz, A., Spelten, N., Konopka, P., Müller, R., Forbes, R.M. and Wernli, H.: Comparison of
786 Fast In situ Stratospheric Hygrometer (FISH) measurements of water vapor in the upper
787 troposphere and lower stratosphere (UTLS) with ECMWF (re) analysis data, *Atm.*
788 *Chem. Phys.*, 14, 10803-10822, 2014.
- 789 Lahoz, W. A., Geer, A. J., Bekki, S., Bormann, N., Ceccherini, S., Elbern, H., Errera, Q.,
790 Eskes, H. J., Fonteyn, D., Jackson, D. R., Khatatov, B., Marchand, M., Massart, S.,
791 Peuch, V.-H., Rharmili, S., Ridolfi, M., Segers, A., Talagrand, O., Thornton, H. E., Vik,
792 A. F., and von Clarmann, T.: The Assimilation of Envisat data (ASSET) project, *Atmos.*
793 *Chem. Phys.*, 7, 1773–1796, <http://www.atmos-chem-phys.net/7/1773/2007/>, 2007b.
- 794 Lahoz, W. A., Peuch, V.-H., Orphal, J., Attie, J.-L., Chance, K., Liu, X., Edwards, D., Elbern,
795 H., Flaud, J.-M., Claeysman, M., and El Amraoui, L.: Monitoring Air Quality from space:
796 The case for the geostationary platform, *Bull. Amer. Meteor. Soc.*, pp. 221–233,
797 doi:10.1175/BAMS-D-11-00045.1, 2012.
- 798 Lambert, A., et al. (2007), Validation of the Aura Microwave Limb Sounder middle
799 atmosphere water vapor and nitrous oxide measurements, *J. Geophys. Res.*, 112,
800 D24S36, doi:10.1029/2007JD008724.



- 801 Liu, C. and Zipser, E. J.: Implications of the day versus night differences of water vapor,
802 carbon monoxide, and thin cloud observations near the tropical tropopause, *J. Geophys.*
803 *Res.*, 114, D09303, doi:10.1029/2008JD011524, 2009.
- 804 Livesey, N. J., W. G. Read, L. Froidevaux, A. Lambert, G. L. Manney, H. C. Pumphrey, M.
805 L. Santee, M. J. Schwartz, S. Wang, R. E. Cofeld, D. T. Cuddy, R. A. Fuller, R. F.
806 Jarnot, J. H. Jiang, B. W. Knosp, P. C. Stek, P. A. Wagner, and D. L. Wu, 2011: Earth
807 Observing System (EOS), Aura Microwave Limb Sounder (MLS), version 3.3 level 2
808 data quality and description document. Jet Propulsion Laboratory, California Institute of
809 Technology, Pasadena, California, USA, available at [http://mhs.jpl.nasa.gov/data/v3-](http://mhs.jpl.nasa.gov/data/v3-3_data_quality_document.pdf)
810 [3_data_quality_document.pdf](http://mhs.jpl.nasa.gov/data/v3-3_data_quality_document.pdf).
- 811 Luo, Z., Kley, D., Johnson, R.H. and Smit, H.: Ten years of measurements of tropical upper-
812 tropospheric water vapor by MOZAIC. Part I: Climatology, variability, transport, and
813 relation to deep convection, *Journal of climate*, 20, 418-435, 2007.
- 814 Milz, M., von Clarmann, T., Fischer, H., Glatthor, N., Grabowski, U., Hopfner, M.,
815 Kellmann, S., Kiefer, M., Linden, A., Mengistu Tsidu, G., Steck, T., Stiller, G. P.,
816 Funke, B., Lopez-Puertas, M., and Koukouli, M. E.: Water Vapor Distributions
817 Measured with the Michelson Interferometer for Passive Atmospheric Sounding on
818 board Envisat (MIPAS/Envisat), *J. Geophys. Res.*, 110, D24307,
819 doi:10.1029/2005JD005973, 2005.
- 820 Oikonomou, E. K. and O'Neill, A.: Evaluation of ozone and water vapor fields from the
821 ECMWF reanalysis ERA-40 during 1991–1999 in comparison with UARS satellite and
822 MOZAIC aircraft observations, *Journal of Geophysical Research: Atmospheres*,
823 111(D14), 2006.



- 824 Panwar, V., Jain, A. R., Goel, A., Mandal, T. K., Rao, V. R., & Dhaka, S. K. (2012). Some
825 features of water vapor mixing ratio in tropical upper troposphere and lower
826 stratosphere: Role of convection. *Atmospheric Research*, 108, 86-103.
- 827 Payra, S., P. Ricaud, R. Abida, J.-L. Attié, L. El Amraoui, F. Carminati, E. Rivière, J.-P.
828 Pommereau, S. Khaykin, Assimilation of water vapour measurements by a Chemistry
829 Transport Model in the tropical UTLS, WWOSC, Montreal, Canada, August 2014.
- 830 Peuch, V. H., Amodei, M., Barthet, T., Cathala, M. L., Josse, B., Michou, M., & Simon, P. :
831 MoCAGE. In Modele de Chimie Atmosphérique aGrande Echelle, paper presented at
832 the Workshop on Atmospheric Modelling, Météo France, Toulouse, France, Dec, 1999.
- 833 Rabier, F., Bouchard, A., Brun, E., Doerenbecher, A., Guedj, S., Guidard, V., Karbou, F.,
834 Peuch, V., El Amraoui, L., Puech, D., Genthon, C., Picard, G., Town, M., Hertzog, A.,
835 Vial, F., Cocquerez, P., Cohn, S., Hock, T., Fox, J., Cole, H., Parsons, D., Powers, J.,
836 Romberg, K., VanAndel, J., Deshler, T., Mercer, J., Haase, J., Avallone, L., Kalnajs, L.,
837 Mechoso, C., Tangborn, A., Pellegrini, A., Frenot, Y., Thpaut, J., McNally, A.,
838 Balsamo, G., and Steinle, P.: The Concordiasi Project in Antarctica, Bull. Amer.
839 Meteor. Soc., 91, 69–86, doi:10.1175/2009BAMS2764.1, 2010.
- 840 Randel, W. J. and Jensen, E. J.: Physical Processes in the tropical tropopause layer and Their
841 roles in a changing climate, *Nature Geoscience*, 6(3), 169-176, 2013.
- 842 Randerson, J.T., G.R. van der Werf, L. Giglio, G.J. Collatz, and P.S. Kasibhatla, Global Fire
843 Emissions Database, Version 3 (GFEDv3.1). Data set. Oak Ridge National Laboratory
844 Distributed Active Archive Center, Oak Ridge, Tennessee, USA, 2013.
845 <http://dx.doi.org/10.3334/ORNLDAAC/1191>
- 846 Read, W.G., A. Lambert, J. Bacmeister, R.E. Cofield, L.E. Christensen, D.T. Cuddy, W.H.
847 Daffer, B.J. Drouin, E. Fetzer, L. Froidevaux, R. Fuller, R. Herman, R.F. Jarnot, J.H.
848 Jiang, Y.B. Jiang, K. Kelly, B.W. Knosp, H.C. Pumphrey, K.H. Rosenlof, X.



- 849 Sabounchi, M.L. Santee, M.J. Schwartz, W.V. Snyder, P.C. Stek, H. Su, L.L. Takacs,
850 R.P. Thurstans, H. Vomel, P.A. Wagner, J.W. Waters, C.R. Webster, E.M. Weinstock,
851 D.L. Wu, "Aura Microwave Limb Sounder upper tropospheric and lower stratospheric
852 H₂O and relative humidity with respect to ice validation", *Journal of Geophysical*
853 *Research* 112, D24S35, doi:10.1029/2007JD008752, 2007.
- 854 Ricaud, P., B. Sič, L. El Amraoui, J.-L. Attié, R. Zbinden, P. Huszar, S. Szopa, J. Parmentier,
855 N. Jaidan, M. Michou, R. Abida, F. Carminati, D. Hauglustaine, T. August, J. Warner,
856 R. Imasu, N. Saitoh, and V.-H. Peuch: Impact of the Asian monsoon anticyclone on the
857 variability of mid-to-upper tropospheric methane above the Mediterranean Basin,
858 *Atmos. Chem. Phys.*, 14, 11427-11446, 2014, doi:10.5194/acp-14-11427-2014.
- 859 Schäfler, A., Dörnbrack, A., Kiemle, C., Rahm, S. and Wirth, M.: Tropospheric water vapor
860 transport as determined from airborne lidar measurements, *Journal of Atmospheric and*
861 *Oceanic Technology*, 27(12), pp.2017-2030, 2010.
- 862 Schiller, C., Groß, J.U., Konopka, P., Plöger, F., Silva dos Santos, F.H. and Spelten, N.:
863 Hydration and dehydration at the tropical tropopause, *Atmos. Chem. Phys.*, 9, 9647-
864 9660, 2009.
- 865 Seinfeld, J. H., and Pandis, S. N., *Atmospheric Chemistry and Physics: From Air Pollution to*
866 *Climate Change*, 2nd ed., John Wiley & Sons, New York, 2006.
- 867 Semane, N., Peuch, V.-H., El Amraoui, L., Bencherif, H., Massart, S., Cariolle, D., Attié, J.-
868 L., and Abida, R.: An observed and analysed stratospheric ozone intrusion over the high
869 Canadian Arctic UTLS region during the summer of 2003, *Quart. J. Roy. Meteor. Soc.*,
870 133, 171–178, 2007.
- 871 SPARC WAVAS (2000), Upper tropospheric and stratospheric water vapour, D. Kley, J. M.
872 Russell III, and C. Phillips (Eds.), WMO/TD-No. 1043, SPARC Rep. No. 2.



- 873 SPARC CCMVal (2010), SPARC report on the evaluation of chemistry climate models, V.
874 Eyring, T. G. Shepherd, D. W. Waugh (Eds.), SPARC Rep. No. 5, WCRP-132,
875 WMO/TD-No. 1526.
- 876 Stiller, G. P., Kiefer, M., Eckert, E., von Clarmann, T., Kellmann, S., Garc'ia-Comas, M.,
877 Funke, B., Leblanc, T., Fetzer, E., Froidevaux, L., Gomez, M., Hall, E., Hurst, D.,
878 Jordan, A., Kampfer, N., Lambert, A., McDermid, I. S., McGee, T., Miloshevich, L.,
879 Nedoluha, G., Read, W., Schneider, M., Schwartz, M., Straub, C., Toon, G., Twigg, L.
880 W., Walker, K., and Whiteman, D. N.: Validation of MIPAS IMK/IAA temperature,
881 water vapor, and ozone profiles with MOHAVE-2009 campaign measurements, Atmos.
882 Meas. Tech., 5, 289–320, doi:10.5194/amt-5-289-2012, 2012.
- 883 Tschanz, B., Straub, C., Scheiben, D., Walker, K. A., Stiller, G. P., and Kämpfer, N.:
884 Validation of middle-atmospheric campaignbased water vapour measured by the
885 ground-based microwave radiometer MIAWARA-C, Atmos. Meas. Tech., 6, 1725–
886 1745, doi:10.5194/amt-6-1725-2013, 2013.
- 887 Uma, K. N., Das, S. K., and Das, S. S., A climatological perspective of water vapor at the
888 UTLS different area over global monsoon regions: observations inferred from the Aura-
889 MLS and reanalysis data, *Climate Dynamics*, 43 (1-2), 407-420, 2014.
- 890 von Clarmann, T., Hopfner, M., Kellmann, S., Linden, A., Chauhan, S., Funke, B.,
891 Grabowski, U., Glatthor, N., Kiefer, M., Schieferdecker, T., Stiller, G. P., and Versick,
892 S.: Retrieval of temperature, H₂O, O₃, HNO₃, CH₄, N₂O, ClONO₂ and ClO from
893 MIPAS reduced resolution nominal mode limb emission measurements, Atmos. Meas.
894 Tech., 2, 159–175, doi:10.5194/amt-2-159- 2009, 2009.
- 895 Waters, J. W., L. Froidevaux, R. S. Harwood, R. F. Jarnot, H. M. Pickett, W. G. Read, P. H.
896 Siegel, R. E. Cofield, M. J. Filipiak, D. A. Flower, J. R. Holden, G. K. Lau, N. J.
897 Livesey, G. L. Manney, H. C. Pumphrey, M. L. Santee, D. L. Wu, D. T. Cuddy, R. R.



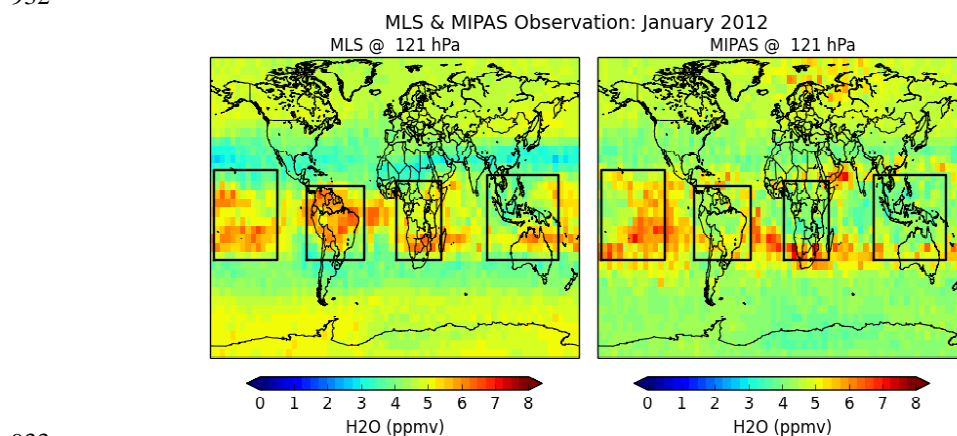
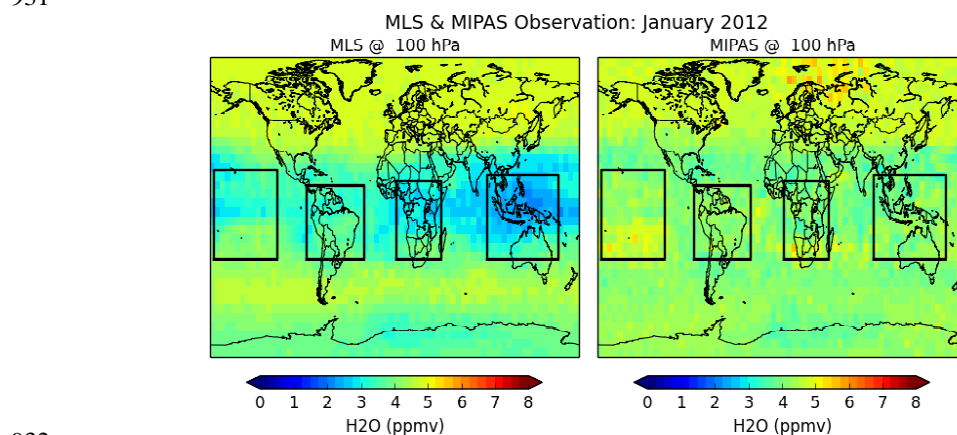
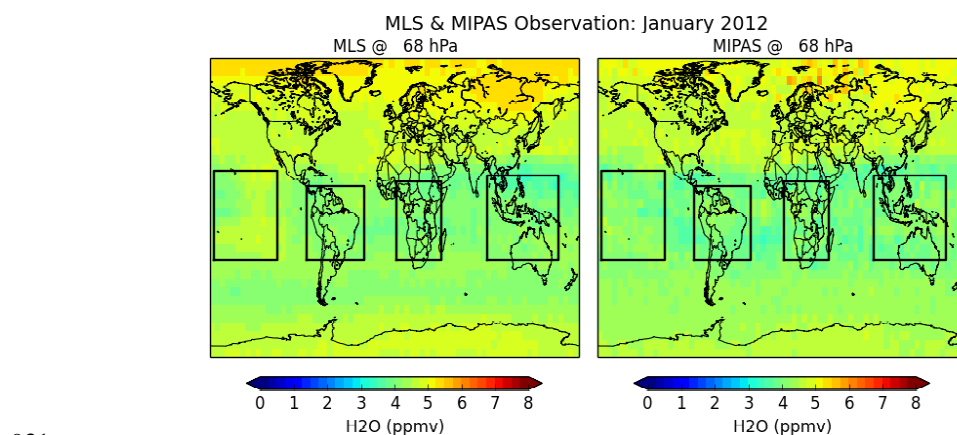
- 898 Lay, M. S. Loo, V. S. Perun, M. J. Schwartz, P. C. Stek, R. P. Thurstans, M. A. Boyles,
899 K. M. Chandra, M. C. Chavez, G. S. Chen, B. V. Chudasama, R. Dodge, R. A. Fuller,
900 M. A. Girard, J. H. Jiang, Y. Jiang, B. W. Knosp, R. C. LaBelle, J. C. Lam, K. A. Lee,
901 D. Miller, J. E. Oswald, N. C. Patel, D. M. Pukala, O. Quintero, D. M. Scaff, W. Van
902 Snyder, M. C. Tope, P. A. Wagner, and M. J. Walch., 2006: The Earth Observing
903 System Microwave Limb Sounder (EOS MLS) on the Aura satellite. IEEE Trans.
904 Geosci. Remote Sensing, 44, 1075-1092, doi: 10.1109/TGRS.2006.873771.
- 905 Weaver, A., and Courtier, P.: Correlation modelling on the sphere using a generalized
906 diffusion equation. Quarterly Journal of the Royal Meteorological Society, 127(575),
907 1815-1846, 2001.
- 908 Weinstock, E. M., et al. (2009), Validation of the Harvard Lyman- α in situ water vapor
909 instrument: Implications for the mechanisms that control stratospheric water vapor, J.
910 Geophys. Res., 114, D23301, doi:10.1029/2009JD012427.
- 911 Wetzel, G., Oelhaf, H., Berthet, G., Bracher, A., Cornacchia, C., Feist, D. G., Fischer, H., Fix,
912 A., Iarlori, M., Kleinert, A., Lengel, A., Milz, M., Mona, L., Müller, S. C., Ovarlez, J.,
913 Pappalardo, G., Piccolo, C., Raspollini, P., Renard, J.-B., Rizi, V., Rohs, S., Schiller, C.,
914 Stiller, G., Weber, M., and Zhang, G.: Validation of MIPAS-ENVISAT H₂O
915 operational data collected between July 2002 and March 2004, Atmos. Chem. Phys., 13,
916 5791–5811, doi:10.5194/acp-13-5791-2013, 2013.
- 917 Yushkov, V., Merkulov, S., and Astakhov, V.: Optical balloon hygrometer for upper
918 stratosphere and stratosphere water vapour measurements, in: Optical remote sensing of
919 the atmosphere and clouds, edited by: Wang, J., Wu, B., Ogawa, T., and Guans, Z.-H.,
920 Proc. SPIE, 3501, 439–445, 1998.
- 921 Zöger, M., Afchine, A., Eicke, N., Gerhards, M.T., Klein, E., McKenna, D.S., Mörschel, U.,
922 Schmidt, U., Tan, V., Tuitjer, F. and Woyke, T.: Fast in situ stratospheric hygrometers:



923 A new family of balloon-borne and airborne Lyman α photofragment fluorescence
924 hygrometers, Journal of Geophysical Research: Atmospheres, 104, 1807-1816, 1999.
925
926
927
928
929
930

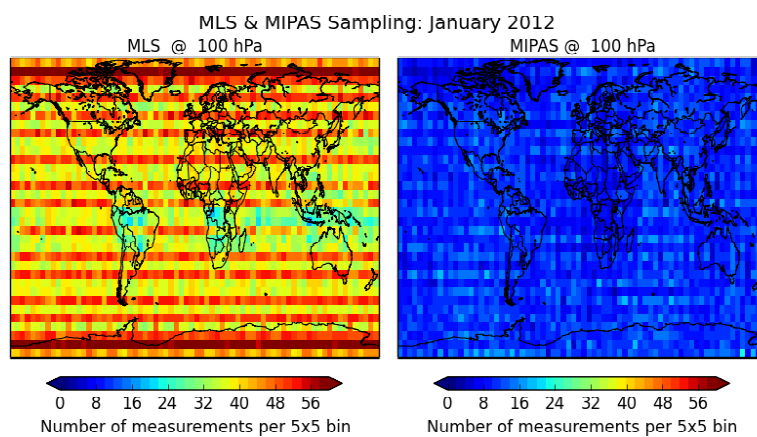


930 **Figure Captions**





934 **Figure 1:** (Upper panel) Monthly-averaged H₂O fields at 68 hPa in January 2012 in the MLS
935 (left) and MIPAS (right) observation space (in space and time coincidence with MLS and
936 MIPAS observations, respectively). (Middle Panel) Same as the upper panel but at 100 hPa.
937 (Lower Panel) Same as the upper panel but at 121 hPa.
938
939



939

940 **Figure 2:** Number of measurements averaged within $5^{\circ} \times 5^{\circ}$ bins at 100 hPa in January 2012

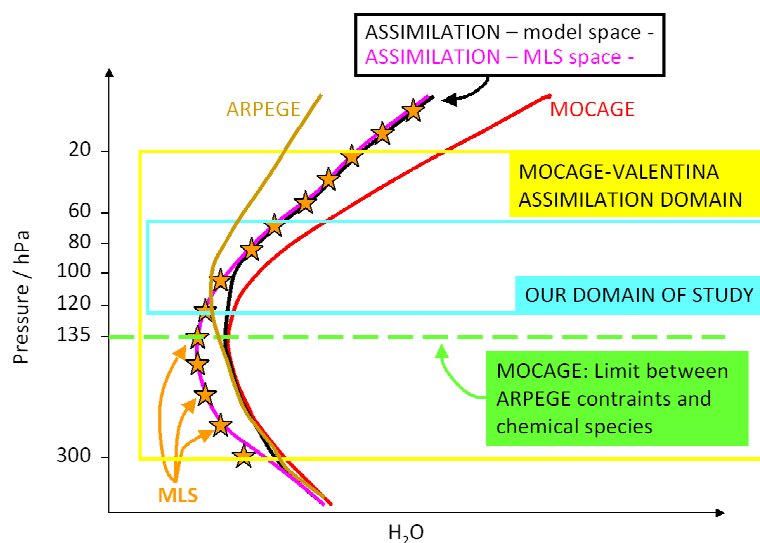
941 in the MLS (left) and MIPAS (right) data sets.

942



942

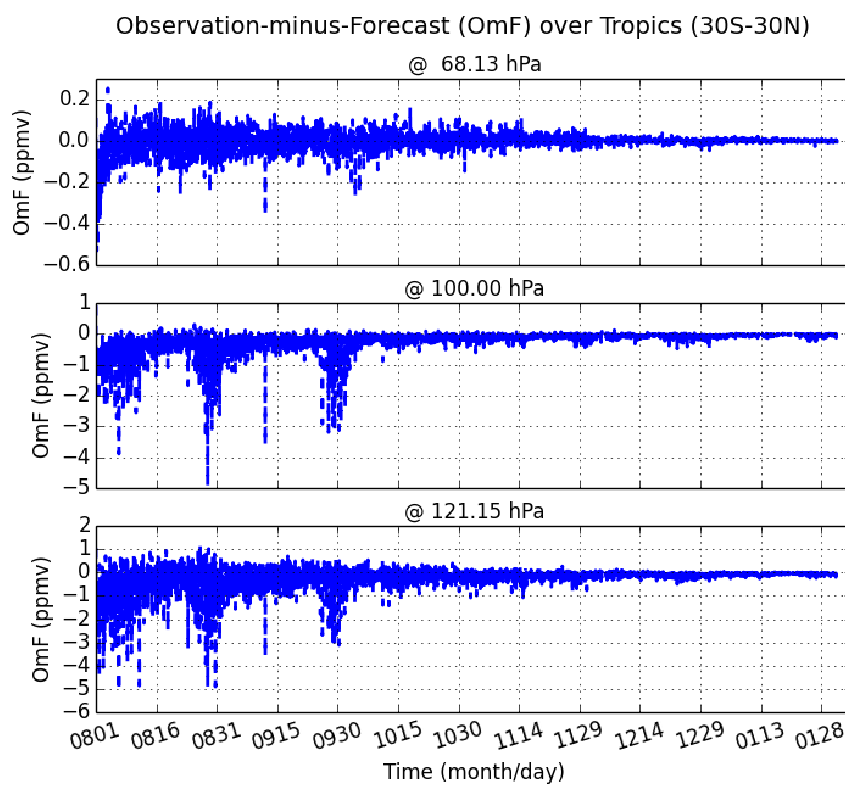
943



944

945 **Figure 3:** Schematic representation of the H_2O vertical profiles used in the present analysis:
946 MLS (orange stars), MOCAGE (red line), ARPEGE (green line), assimilation in the MLS
947 space (in time and space coincidence with MLS observations, pink line), and assimilation in
948 the model space (in time and space coincidence with the model outputs, purple line). In
949 MOCAGE, H_2O is constrained to ARPEGE meteorological analyses below 135 hPa
950 (horizontal dashed green line) and is considered as a chemical species above 135 hPa. MLS
951 observations are assimilated from 300 to 20 hPa. Our domain of study relies from 121 to 68
952 hPa in the tropics.

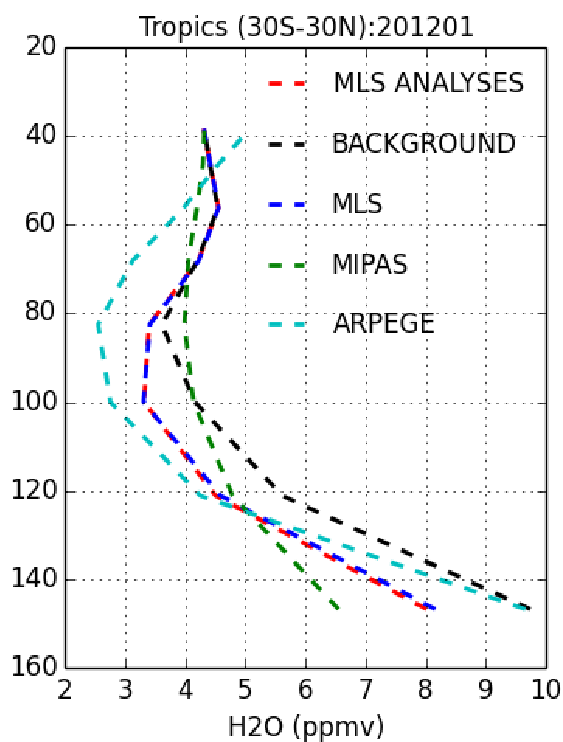
953



953

954 **Figure 4:** Observations minus forecasts zonally averaged over the tropics (30°S-30°N) from
955 1 August 2011 to 31 January 2012 at 121 hPa (bottom), 100 hPa (middle) and 68 hPa (top).

956

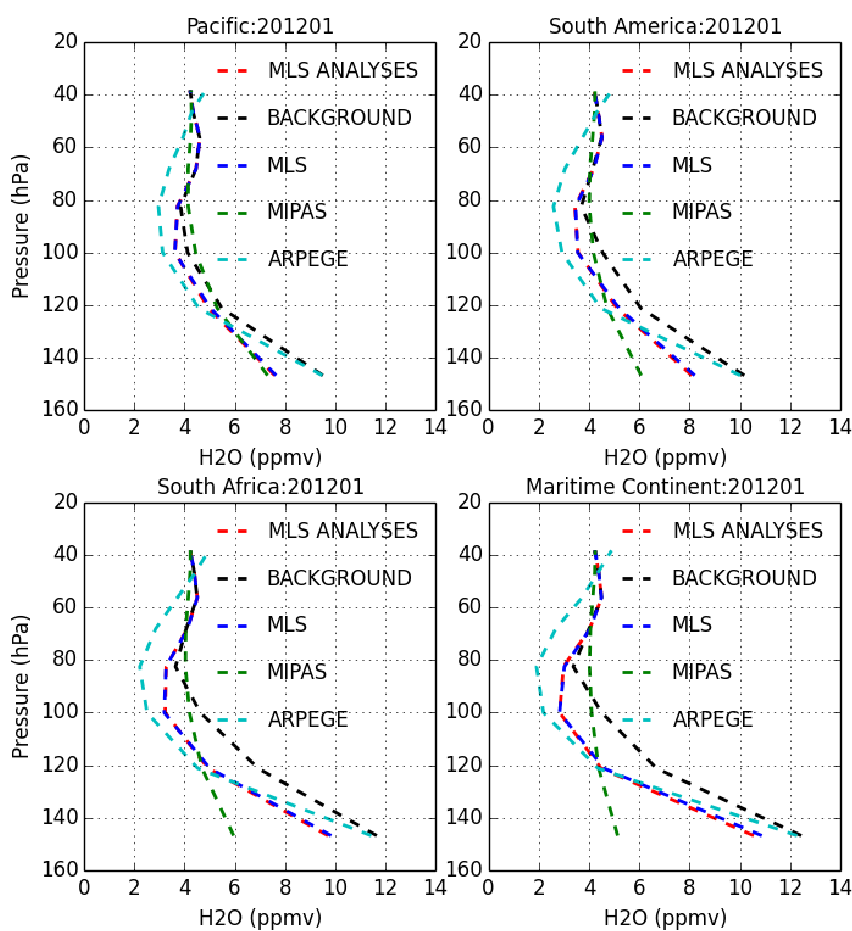


956

957 **Figure 5:** Monthly-averaged vertical profiles of H₂O in the tropical UTLS (30°S-30°N) in
958 January 2012 in the MLS observation space from MLS analyses (red dashed line),
959 Background (black dashed line), MLS (blue dashed line), MIPAS (green dashed line) and
960 ARPEGE (light blue line).

961

962



962

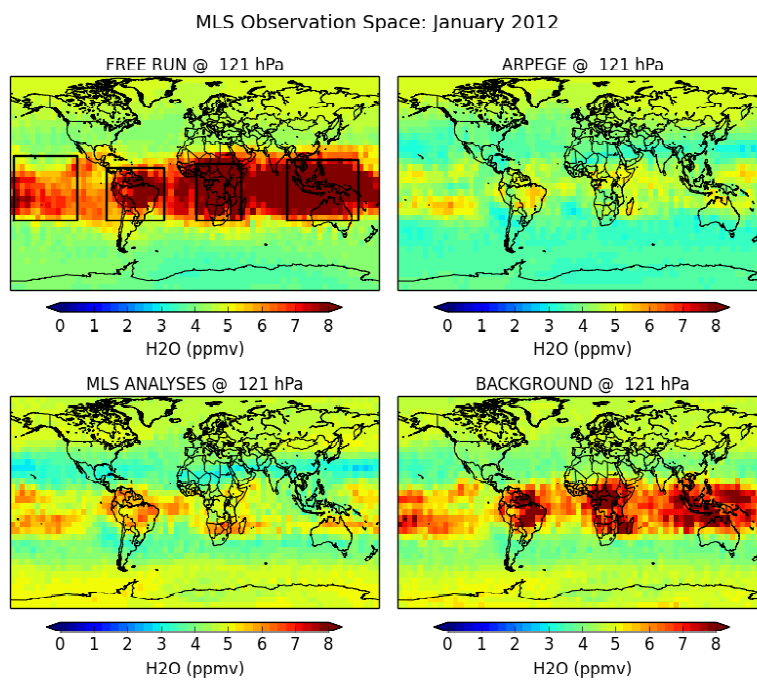
963 **Figure 6:** Monthly-averaged vertical profiles of H₂O in January 2012 in the MLS observation
964 space from MLS analyses (red dashed line), Background (black dashed line), MLS (blue
965 dashed line), MIPAS (green dashed line) and ARPEGE (light blue line) in four different
966 tropical areas (see Figure 1): Pacific Ocean (upper left), South America (upper right), South
967 Africa (lower left) and Maritime Continent (lower right).

968

969



969



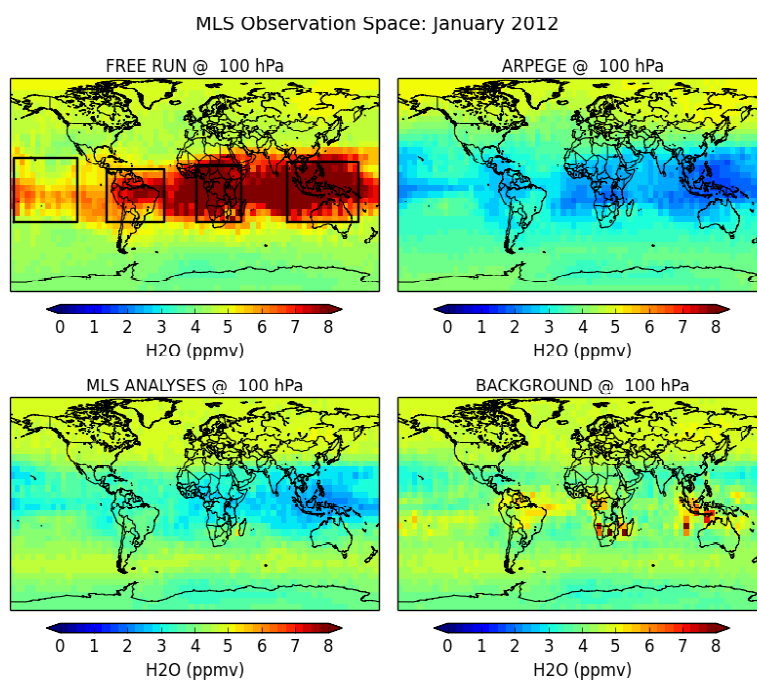
970

971 **Figure 7:** Monthly-averaged H₂O fields at 121 hPa in January 2012 in the MLS observation
972 space (in time and space coincidence with MLS observations) from the Free Run (MOCAGE,
973 upper left), ARPEGE (upper right), MLS analyses (assimilation, lower left) and the
974 background (lower right).

975

976

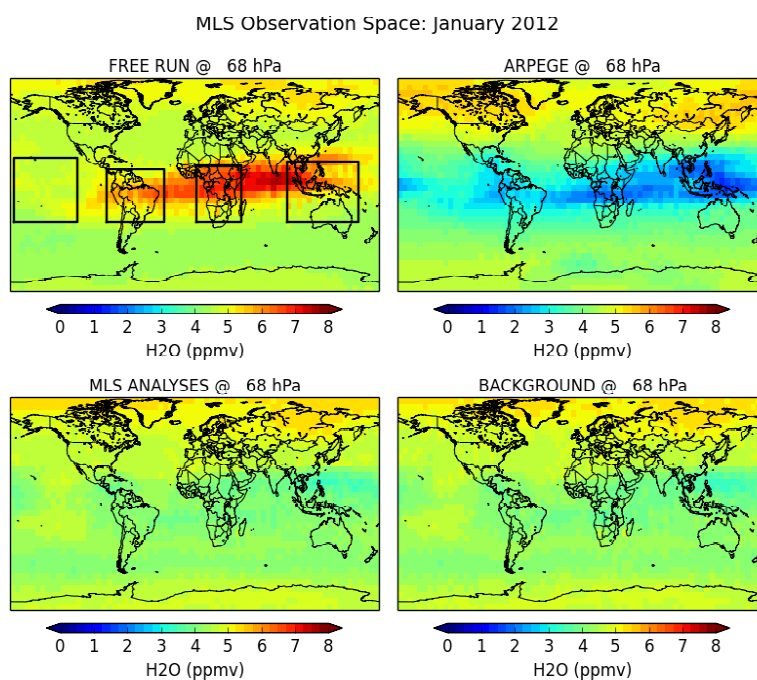
977



977

978 **Figure 8:** Monthly-averaged H₂O fields at 100 hPa in January 2012 in the MLS observation
979 space (in time and space coincidence with MLS observations) from the Free Run (MOCAGE,
980 upper left), ARPEGE (upper right), MLS analyses (assimilation, lower left) and the
981 background (lower right).

982

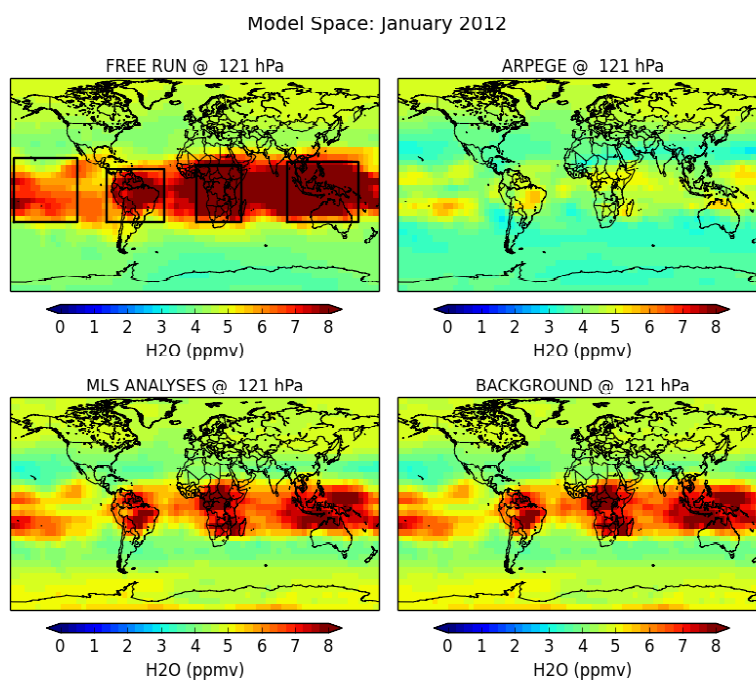


982

983 **Figure 9:** Monthly-averaged H₂O fields at 68 hPa in January 2012 in the MLS observation
984 space (in time and space coincidence with MLS observations) from the Free Run (MOCAGE,
985 upper left), ARPEGE (upper right), MLS analyses (assimilation, lower left) and the
986 background (lower right).

987

988



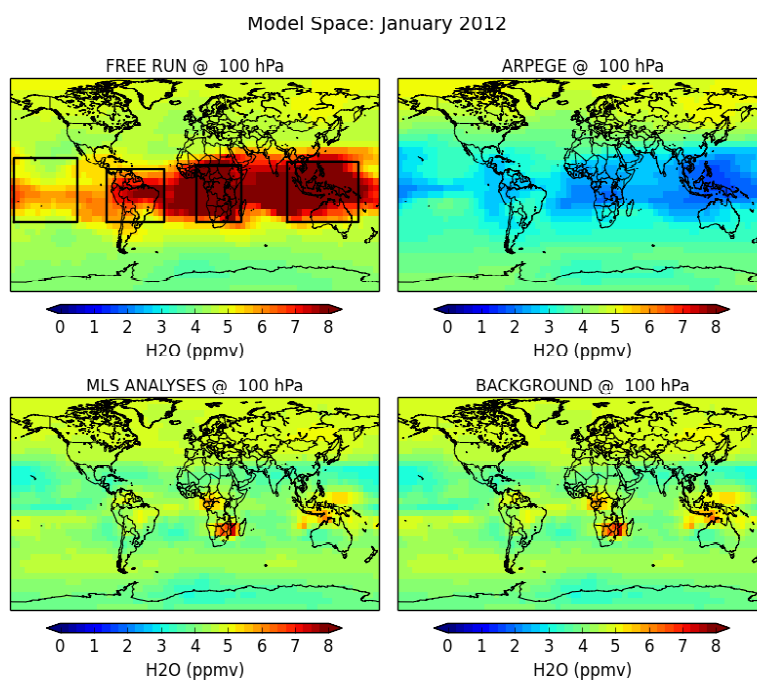
988

989 **Figure 10:** Monthly-averaged H₂O fields at 121 hPa in January 2012 in the Model space (in
990 the Model grid and time samplings) from the Free Run (MOCAGE, upper left), ARPEGE
991 (upper right), MLS analyses (assimilation, lower left) and the background (lower right).

992

993

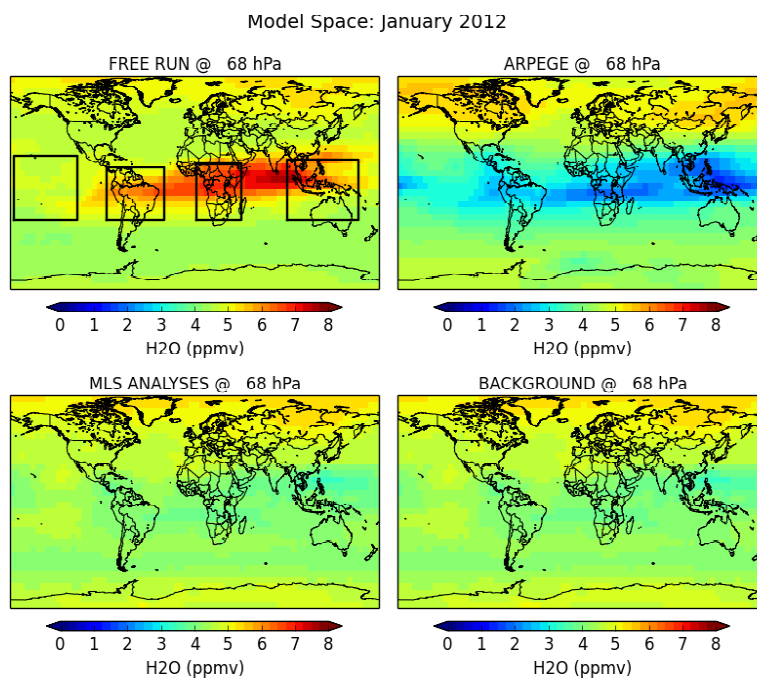
994



994

995 **Figure 11:** Monthly-averaged H₂O fields at 100 hPa in January 2012 in the Model space (in
996 the Model grid and time samplings) from the Free Run (MOCAGE, upper left), ARPEGE
997 (upper right), MLS analyses (assimilation, lower left) and the background (lower right).

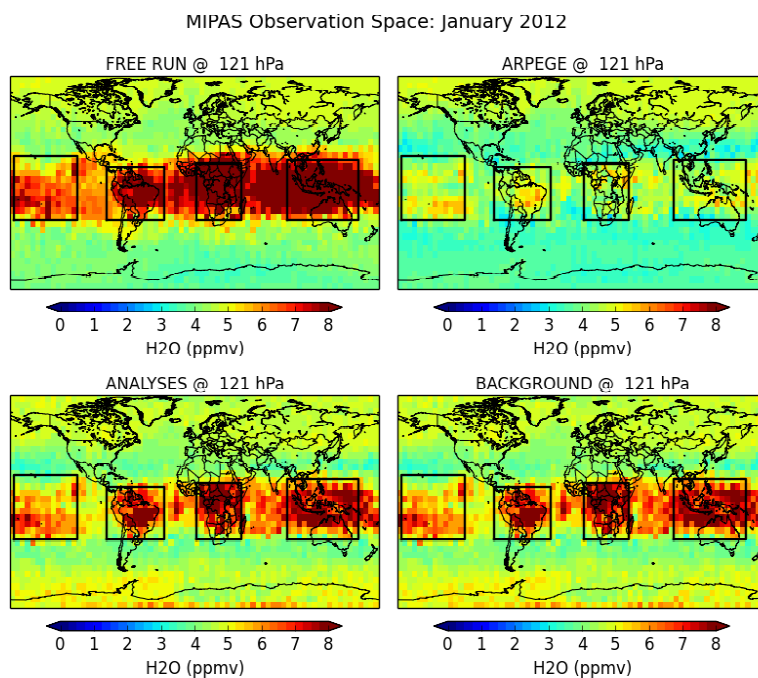
998



999

1000 **Figure 12:** Monthly-averaged H₂O fields at 68 hPa in January 2012 in the Model space (in
1001 the Model grid and time samplings) from the Free Run (MOCAGE, upper left), ARPEGE
1002 (upper right), MLS analyses (assimilation, lower left) and the background (lower right).

1003

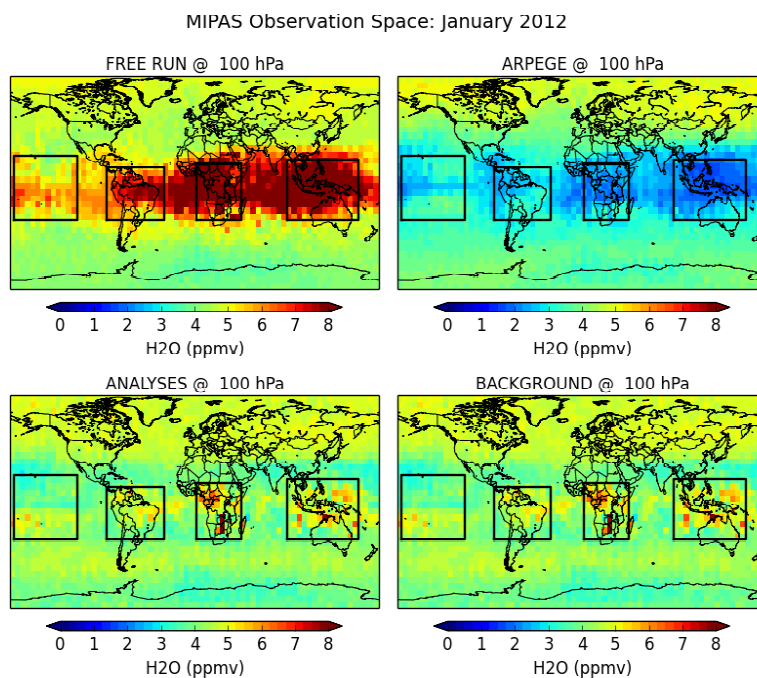


1003

1004 **Figure 13:** Monthly-averaged H₂O fields at 121 hPa in January 2012 in the MIPAS
1005 observation space (in time and space coincidence with MIPAS observations) from the Free
1006 Run (MOCAGE, upper left), ARPEGE (upper right), MLS analyses (assimilation, lower left)
1007 and the background (lower right).

1008

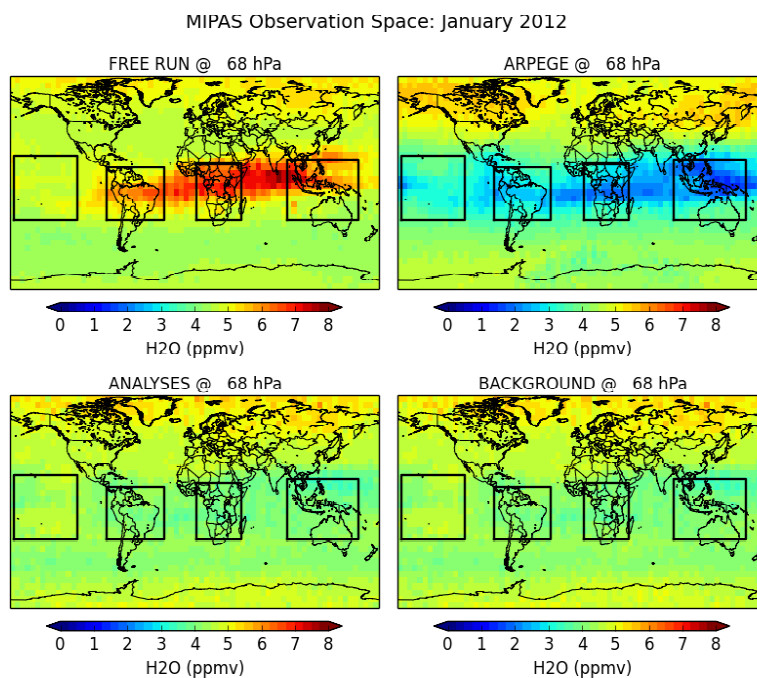
1009



1009

1010 **Figure 14:** Monthly-averaged H₂O fields at 100 hPa in January 2012 in the MIPAS
1011 observation space (in time and space coincidence with MIPAS observations) from the Free
1012 Run (MOCAGE, upper left), ARPEGE (upper right), MLS analyses (assimilation, lower left)
1013 and the background (lower right).

1014

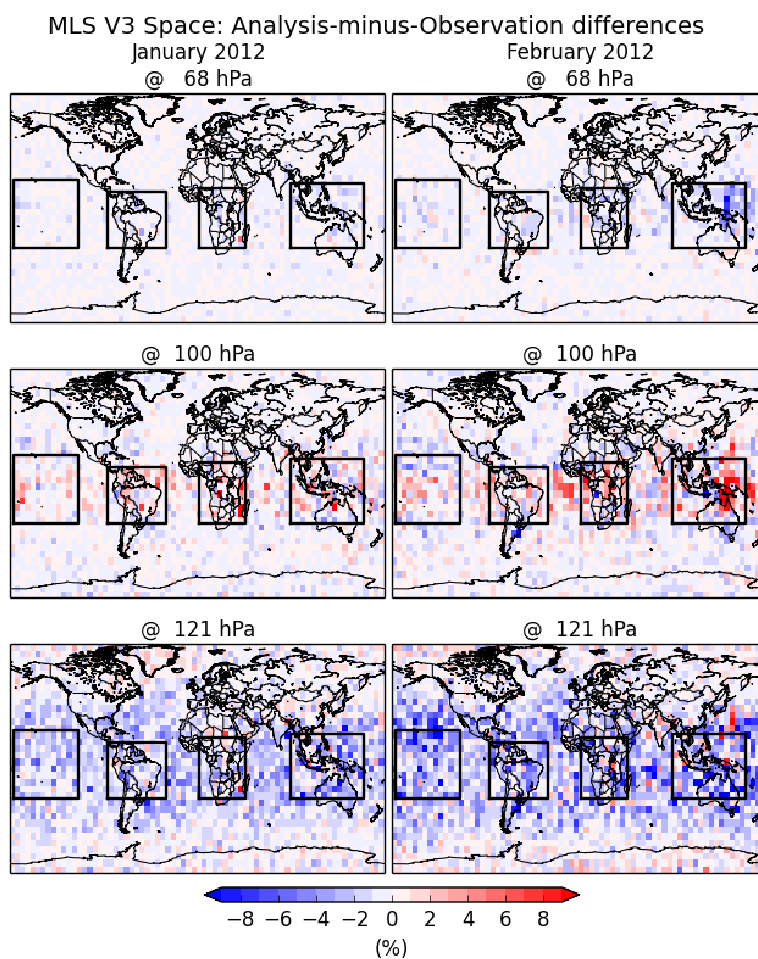


1014

1015 **Figure 15:** Monthly-averaged H₂O fields at 68 hPa in January 2012 in the MIPAS observation space (in
1016 time and space coincidence with MIPAS observations) from the Free Run (MOCAGE, upper left),
1017 ARPEGE (upper right), MLS analyses (assimilation, lower left) and the background (lower right).

1018

1019

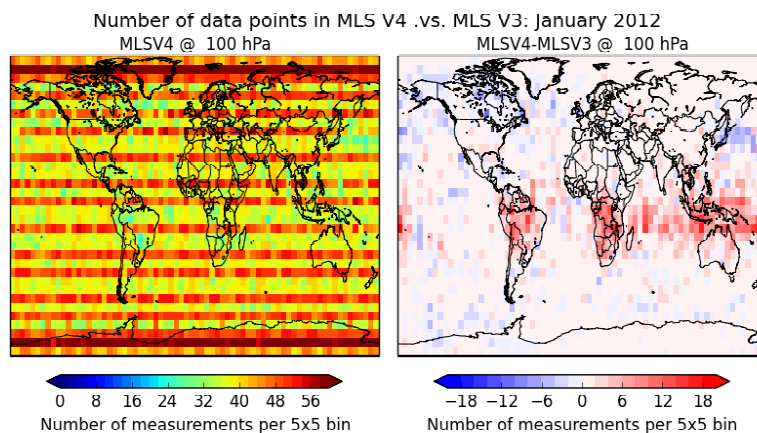


1019

1020 **Figure 16:** Relative difference between the H₂O fields from the observation and the
1021 assimilation in January 2012 (left) and in February 2012 (right) at 121 hPa (bottom), 100 hPa
1022 (middle) and 68 hPa (top).

1023

1024



1024

1025 **Figure 17:** Number of measurements averaged within $5^{\circ} \times 5^{\circ}$ bins at 100 hPa in January 2012
1026 in the MLS V4 data set (left). Difference between the number of measurements averaged
1027 within $5^{\circ} \times 5^{\circ}$ bins at 100 hPa in January 2012 in the MLS V4 and the MLS V3 data sets
1028 (right).

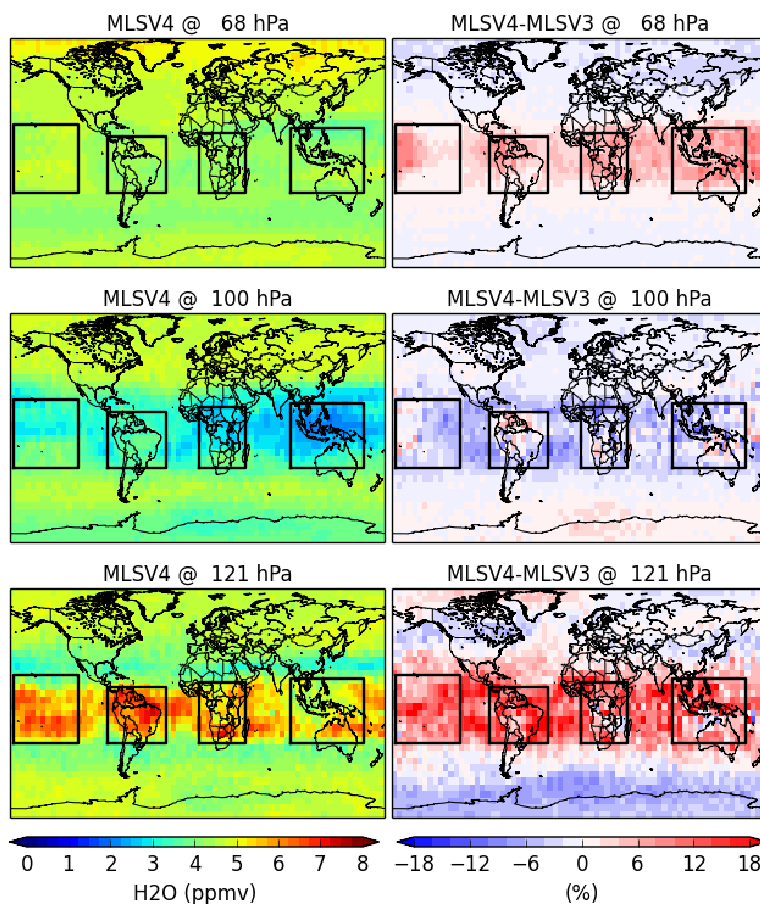
1029

1030

1031



MLS V4 vs. MLS V3: January 2012



1031

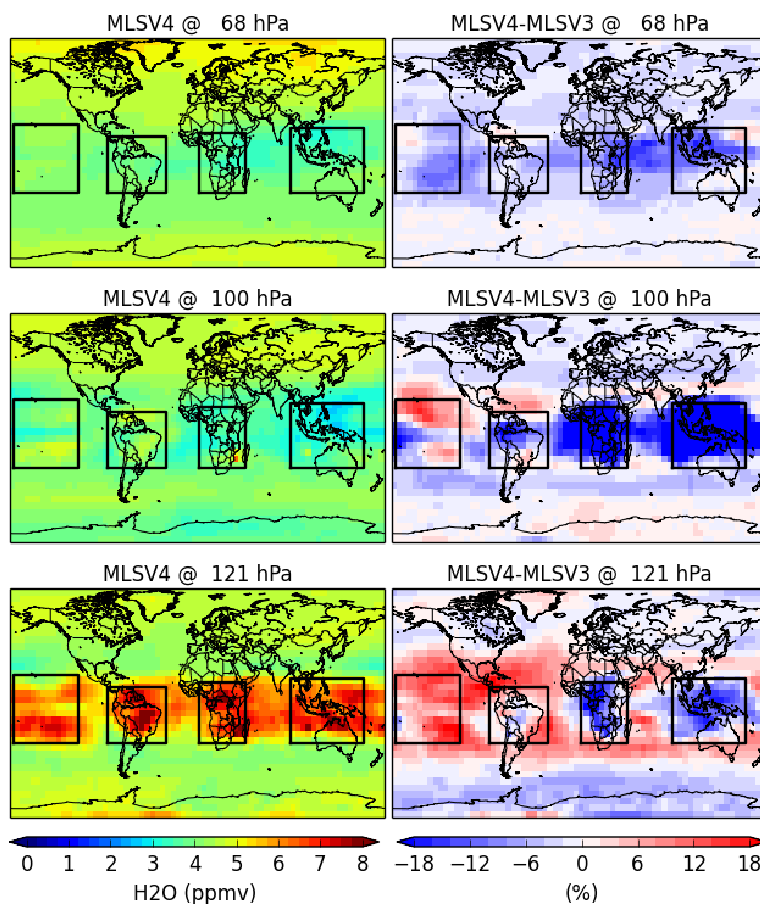
1032 **Figure 18:** Monthly-averaged H₂O analyses in the MLS space in January 2012 using the
1033 MLS V4 data set (left) and relative difference between the MLS analyses using V4 and V3
1034 data sets (right) at 121 hPa (bottom), 100 hPa (middle) and 68 hPa (top).

1035

1036



Model Analyses/MLS V4 vs. MLS V3: January 2012



1036

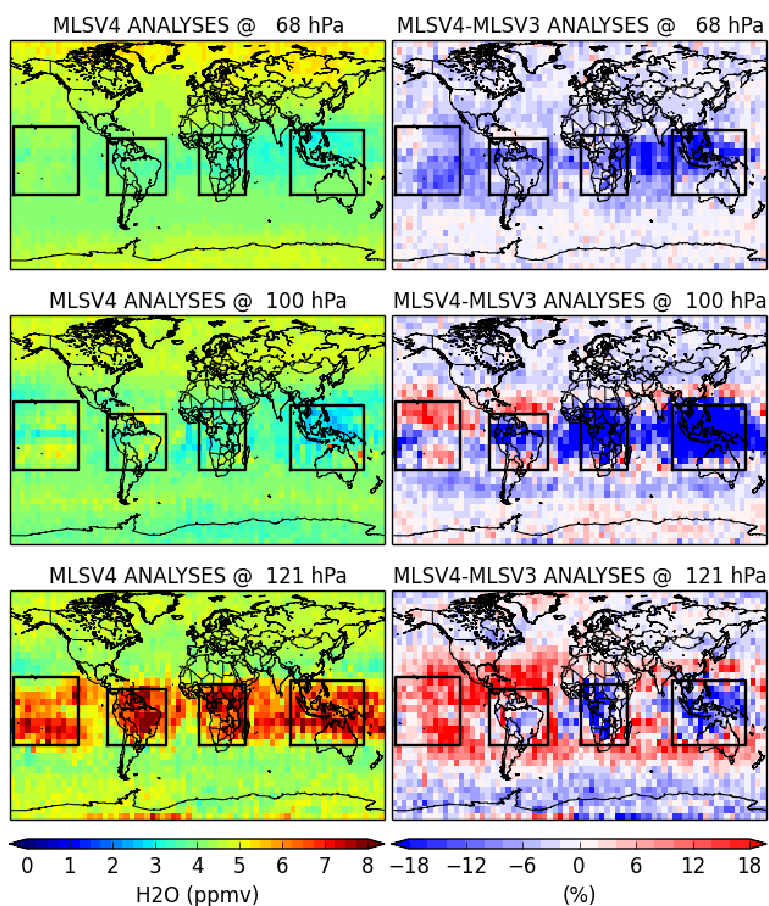
1037 **Figure 19:** Monthly-averaged H₂O analyses in the model space in January 2012 using the
1038 MLS V4 data set (left) and relative difference between the MLS analyses using V4 and V3
1039 data sets (right) at 121 hPa (bottom), 100 hPa (middle) and 68 hPa (top).

1040

1041



MLSV3 & MLSV4 Analyses in MIPAS Space: January 2012



1041

1042 **Figure 20:** Monthly-averaged H₂O analyses in the MIPAS space in January 2012 using the
1043 MLS V4 data set (left) and relative difference between the MLS analyses using V4 and V3
1044 data sets (right) at 121 hPa (bottom), 100 hPa (middle) and 68 hPa (top).

1045

1046